Chapter 9

Cloud Ice Properties: In Situ Measurement Challenges

D. BAUMGARDNER,[a] S. J. ABEL,[b] D. AXISA,[c] R. COTTON,[b] J. CROSIER,[d] P. FIELD,[b] C. GURGANUS,[e] A. HEYMSFIELD,[c] A. KOROLEV,[f] M. KRÄMER,[g] P. LAWSON,[e] G. MCFARQUHAR,[h] Z. ULANOWSKI,[i] AND J. UM[h]

[a] *Droplet Measurement Technologies, Inc., Boulder, Colorado*
[b] *Met Office, Exeter, United Kingdom*
[c] *National Center for Atmospheric Research, Boulder, Colorado*
[d] *University of Manchester, Manchester, United Kingdom*
[e] *Stratton Park Engineering Corporation, Boulder, Colorado*
[f] *Environment Canada, Toronto, Ontario, Canada*
[g] *Forschungszentrum Jülich, Jülich, Germany*
[h] *University of Illinois at Urbana–Champaign, Urbana, Illinois*
[i] *University of Hertfordshire, Hertfordshire, United Kingdom*

ABSTRACT

Understanding the formation and evolution of ice in clouds requires detailed information on the size, shape, mass, and optical properties of individual cloud hydrometeors and their bulk properties over a broad range of atmospheric conditions. Since the 1960s, instrumentation and research aircraft have evolved, providing increasingly more accurate and larger quantities of data about cloud particle properties. In this chapter, the current status of electrical powered, in situ measurement systems are reviewed with respect to their strengths and weaknesses and their limitations and uncertainties are documented. There remain many outstanding challenges. These are summarized and accompanied by recommendations for moving forward through new developments that fill the remaining information gaps. Closing these gaps will remove the obstacles that continue to hinder our understanding of cloud processes in general and the evolution of ice in particular.

1. Chapter overview

Since the early 1960s there have been many cloud physics field programs conducted with instrumented research aircraft. Many of these projects focused on measuring the microphysical properties of ice; however, significant gaps remain in our understanding of fundamental processes. These gaps are primarily a result of the inherent limitations and uncertainties associated with the instruments that make the measurements. Improving our measurement capabilities in order to close these gaps remains a significant challenge for the scientific community.

There are many publications that describe the instruments that are most frequently deployed for in situ measurements of the microphysical properties of clouds (e.g., Baumgardner et al. 2011a,b; Wendisch and Brenguier 2013). These documents provide detailed information on the instrument operating principles but fewer specifics on the sources and magnitudes of operational limitations and uncertainties.

The objective of this chapter is to focus on the problems associated with making measurements with airborne instruments. Table 9-1 lists most of the instruments that are currently in use and have been since the 1980s (some older instruments such as impaction devices are not listed). Table 9-2 summarizes the known uncertainties and limitations of the different measurement techniques that are discussed in the following sections.

The primary objective of this chapter is to bring together, in a single document, a summary of the uncertainties and limitations that are associated with general classes of instruments, complemented by an

Corresponding author e-mail: D. Baumgardner, darrel.baumgardner@gmail.com

DOI: 10.1175/AMSMONOGRAPHS-D-16-0011.1

TABLE 9-1. In situ cloud particle instruments.

Parameter measured	Measurement technique	Instrument	Measurement range	Manufacturer	Primary references
Particle size	Impaction	Video ice particle sampler (VIPS)	5–200 μm	NCAR	Heymsfield and McFarquhar (1996)
	Light scattering and interference	FSSP-100	2–50 μm	Formerly Particle Measuring Systems, Inc. (PMS), no longer available	Knollenberg (1976, 1981)
		Fast FSSP-100 (FFSSP)	1–50 μm	SPEC	www.specinc.com
		CDP	2–50 μm	DMT	Lance et al. (2010)
		FCDP	1–50 μm	SPEC	www.specinc.com
		CAS	0.5–50 μm	DMT	Baumgardner et al. (2001)
		CAS-POL	0.5–50 μm	DMT	Glen and Brooks (2013)
		BCP	5.0–75 μm	DMT	Beswick et al. (2014)
		CPSPD	0.5–50 μm	DMT	Baumgardner et al. (2014)
		SID-2/3	2–70 μm/2–140 μm	University of Hertfordshire	Cotton et al. (2010), Ulanowski et al. (2014)
		Phase Doppler interferometer (PDI)	1–2000 μm	Artium	Bachalo (1980)
		HOLODEC	5–2000 μm	NCAR	Fugal and Shaw (2009)
	Imaging probes	2D-C/2DG	25–800 μm/25–1600 μm	formerly PMS, no longer available	Knollenberg (1970, 1976, 1981)
		2D-P	200–6400 μm	formerly PMS, no longer available	Knollenberg (1970, 1976, 1981)
		260-X	10–620 μm	formerly PMS, no longer available	Knollenberg (1970, 1976, 1981)
		CIP	25–1550 μm	DMT	Baumgardner et al. (2001)
		CIP-GS	15–900 μm	DMT	Baumgardner et al. (2001)
		PIP	100–6400 μm	DMT	Baumgardner et al. (2001)
		CPI	2.3–>2000 μm	SPEC	Lawson et al. (2001)
		2D-S	10–1280 μm	SPEC	Lawson et al. (2006)
		HVPS-3	150–19 200 μm	SPEC	Lawson et al. (1998)
		3V-CPI	4.6–1280 μm	SPEC	www.specinc.com
		PHIPS-HALO	5–800 μm	Karlsruhe Institute of technology (KIT)	Abdelmonem et al. (2011, 2016)
		HSI	5–1250 μm	Artium	http://www.artium.com
Optical properties	Light scattering	PN		Laboratoire de Météorologie Physique (LaMP)	Gayet et al. (1997)
		CIN		Gerber Scientific, Inc. (GSI)	Gerber (2000)
		CEP		Environment and Climate Change Canada (ECCC)	Korolev et al. (2014)
		PHIPS-HALO		KIT	Abdelmonem et al. (2011, 2016)
Water content	Hot wires and evaporators	King LWC probe and LWC-100/300	0.05–3.0 g m^{-3} @ 100 m s^{-1}	Formerly PMS (no longer available), and DMT	King et al. (1978)
		Nevzorov LWC/TWC	0.002–>3.0 g m^{-3} @ 100 m s^{-1}	SkyPhysTech, Inc.	Korolev et al. (1998b)
		TWP	0–20 g kg^{-1}	Met Office	Nicholls et al. (1990)
		HTW isokinetic evaporator	5–2500 ppmv	Harvard University	Weinstock et al. (2006)
		CLH	0.005–1 g m^{-3}	University of Colorado	Davis et al. (2007)
		FISH	0.5–1000 ppmv condensed + vapor	Forschungszentrum Jülich (FSJ)	Schiller et al. (2008)
		CVI	0.003–2 g m^{-3}	NCAR, DMT	Noone et al. (1988)

TABLE 9-1. (*Continued*)

Parameter measured	Measurement technique	Instrument	Measurement range	Manufacturer	Primary references
			@ 100 m s^{-1}		
		IKP	0–10 g m^{-3}	Science Engineering Associates (SEA)	Davison et al. (2009, 2011)
	Light scattering	PVM-100A	0.002–3 g m^{-3}	GSI	Gerber et al. (1994)

extensive bibliography. The discussion of operating principles is limited to what is necessary to understand the nature of the measurement issues. The reader is directed to the references listed in Tables 9-1 and 9-2, and those throughout the text, for more detailed information on the measurement principles of specific instruments.

Although this monograph is devoted to the measurement of ice in clouds, the measurement issues that are discussed are also relevant, in most cases, to the measurement of water droplets and liquid water content (LWC), as well.

A final note concerns the reporting of measurement uncertainties or errors, used here synonymously. The listed uncertainties are taken from numerous publications, not all of which follow the same methodology to derive the measurement error. It is considered good practice to separate estimated errors into systematic (bias) and random errors. What is reported here, however, are the combination of these two types of error, unless otherwise stated.

2. Single-particle detection techniques

a. Light scattering

1) MEASUREMENT PRINCIPLES

The light-scattering sensors currently in use for cloud measurements are the Forward Scattering Spectrometer Probe (FSSP), the Cloud Droplet Probe (CDP), the Cloud and Aerosol Spectrometer (CAS), the Cloud and Aerosol Spectrometer with polarization (CAS-POL), the Fast Cloud Droplet Probe (FCDP), the Backscatter Cloud Probe (BCP), and the Small Ice Detector (SID) family. Figures 9-1a–d illustrate the basic detection system for all instruments except the SID and BCP, which do not use a forward-scattering qualifier; the SID collects light over a broad range of angles using a multielement detector while the BCP collects light over a smaller backscattering range of angles. Light that is scattered from particles passing through a laser beam is directed to detectors, one that measures all the collected light (blue detector, sizer) and the other that has an optical mask that prevents light detection from out-of-focus particles (red, qualifier). When the particle is in the sample area, the qualifier signal exceeds that of the sizer (Fig. 9-1a), whereas the opposite is true when the particle is outside the sample area (Fig. 9-1b). As shown in Fig. 9-1c the collection angles are determined by the distance from the sample plane to the beam dump (L), the radii of the beam dump (R), and the size of the collection aperture (X). The equivalent optical diameter (EOD) is derived from the peak scattering intensity by applying Mie theory, along with scale factors derived from calibrations. The intensity of the collected light is sensitive to these collection angles as illustrated in Fig. 9-1d where a $\pm 0.5°$ change leads to more than $\pm 20\%$ differences in collected light. Although the nominal collection angles of the FSSP, CDP, and FCDP are 4°–12°, as discussed by Hovenac and Hirleman (1991), probe-to-probe variations in the optical mounting can lead to more than $\pm 1°$ in both the inner and outer angles The uncertainties in the collection geometry contribute to the sizing accuracy discussed in the next section. Hereafter, the single-particle instruments will be referred to as on-axis scattering spectrometers (OSS) to differentiate them from the SIDs that collect light over larger angles.

There are several models of the SID that collect scattered light using a multielement main detector over a range of angles from 9° to 20° for SID-2 to 7° to 25° for SID-3 and related implementations. Two trigger detectors at larger scattering angles provide nested sample volumes. The first model had six main detector elements to record the scattering patterns. The later models have had increasingly more elements (see section 4). The definition of the sample volume with overlapping view volumes, and the derivation of the EOD are essentially the same with all models. The EOD is derived by fitting an exponential power-law function to the calibration data, that is, EOD = aS^b, where S is the scattering intensity. The sample area is also determined from laboratory calibrations (Cotton et al. 2010).

The BCP collects backscattered light over the angles from 144° to 156° and has no qualifier optics to define the sample volume. All particles in the view volume are measured and an inversion algorithm is used to derive the size distribution taking into account the nonuniformity in laser intensity.

TABLE 9-2. Measurement limitations and uncertainties.

Measurement technique	Parameter	Limitations and uncertainty sources	Propagated uncertainty
Light scattering	Size	Mie ambiguity, collection angles, coincidence, nonsphericity, shattering	10%–50%
	Concentration	Sample area uncertainty, coincidence, shattering	10%–30%
	Shape	Only SID can derive shape	
Imaging	Size	Out of focus, time response, shattering, discretization	10%–100%
	Concentration	Variable DOF, shattering	10%–100%
	Shape	Requires 5–12 pixels, out-of-focus drops may look nonspherical	
Evaporation	LWC	Dry-air removal, large droplet rolloff, ice crystal response	10%–30%
	TWC	Dry-air removal, bouncing and pooling, saturation	10%–30%
Diffraction	LWC	Large particle rolloff, liquid/ice discrimination	5%–30%

2) SIZING LIMITATIONS AND UNCERTAINTIES

(i) Mie scattering uncertainties

The pattern and intensity of scattered light depends on the particle diameter, shape, orientation (if nonspherical), refractive index, and incident light wavelength. The scattering cross section is determined from Mie theory for a given collection angle and particle diameter, if it is spherical with a known refractive index. Figure 9-2a illustrates the theoretical relationship between water droplet diameter and scattering cross section from 4° to 12° (OSS) and from 9° to 20° (SID-2), both assuming a laser wavelength of 680 nm. The dashed curves are power-law fits to the theoretical values. Figure 9-2b shows the error when deriving the size from the best fit compared to the theoretical size. The errors for spheres are largest, $>\pm 20\%$, below 10 μm, decreasing to $<10\%$ between 10 and 30 μm, and then increasing again at larger sizes. Not only do these oscillations lead to size distributions with unnatural multimodal shapes, but the errors are propagated into the derived median volume diameter (MVD), LWC, and other bulk microphysical properties. Corrective steps that can decrease this uncertainty are discussed in McFarquhar et al. (2017, chapter 11).

As shown in Fig. 9-1d, the sensitivity to changes as small as $\pm 0.5°$ in the collection angle Θ_2 will lead to errors that increase with size. The left axis shows the size thresholds as a function of particle diameter as they would be set up in a nominal probe with forward collection angles from 4° to 12° (blue solid curve). The black and red curves show how they should have been set up if the scattering angles were actually 4°–11.5° or 4°–12.5° (black and red curves, respectively). As illustrated by the box, the sizing error is found by taking the scattering signal counts designated by the blue curve and selecting the same counts on the red or black curve to locate the equivalent size. The dashed curves and right axis show the error in derived diameter. In the case illustrated with the blue box, for a 40-μm EOD, the sizing uncertainty is approximately $\pm 4\,\mu$m, or 10%. Note that the length of the depth of field (DOF) is typically on the order of 0.5 mm, contributing to a variation of approximately $\pm 1°$, or about $\pm 10\%$ in sizing uncertainty. The uncertainty in the collection angles can be greatly decreased by measuring the DOF using the diffraction pattern generated by a pinhole (Hovenac and Hirleman 1991) or mapping the sample area with a stream of monodispersed droplets (Lance et al. 2010). By selecting two or more droplet diameters, the collection angles can also be determined by fitting the scattering cross sections calculated with Mie theory to the measurements.

(ii) Sizing uncertainties related to particle shape

The nonspherical shape of ice crystals presents a major issue for deriving an EOD from the intensity of scattered light. For nonspherical ice crystals the definition of size becomes problematic since, even if capturing the geometric shape with imaging probe (discussed in the following section), the meaning of size is ambiguous (e.g., Wu and McFarquhar 2016). The SIDs measure the pattern of scattered light which allows the discrimination of ice crystals from water droplets (Vochezer et al. 2016; Järvinen et al. 2016) and the probes that measure a polarization signal [CAS-POL, Cloud Particle Spectrometer with Polarization Detection (CPSPD)] can discriminate, to some degree, the nonsphericity (Glen and Brooks 2013; Järvinen et al. 2016). The interpretation of measurements from the light-scattering probes is difficult since the derivation of an EOD assumes sphericity; that is, the EOD is the diameter of a water droplet that would have scattered the same intensity of light, in the respective angular detection range, as the nonspherical particle that was measured. When the particle is quasi-spherical, the resulting EOD will represent the size, within the expected uncertainties, associated with Mie theory (Gayet et al. 1996); however, for more nonspherical particles, the variation in the derived EOD will depend on the aspect ratio and orientation of the particle when in the sample area.

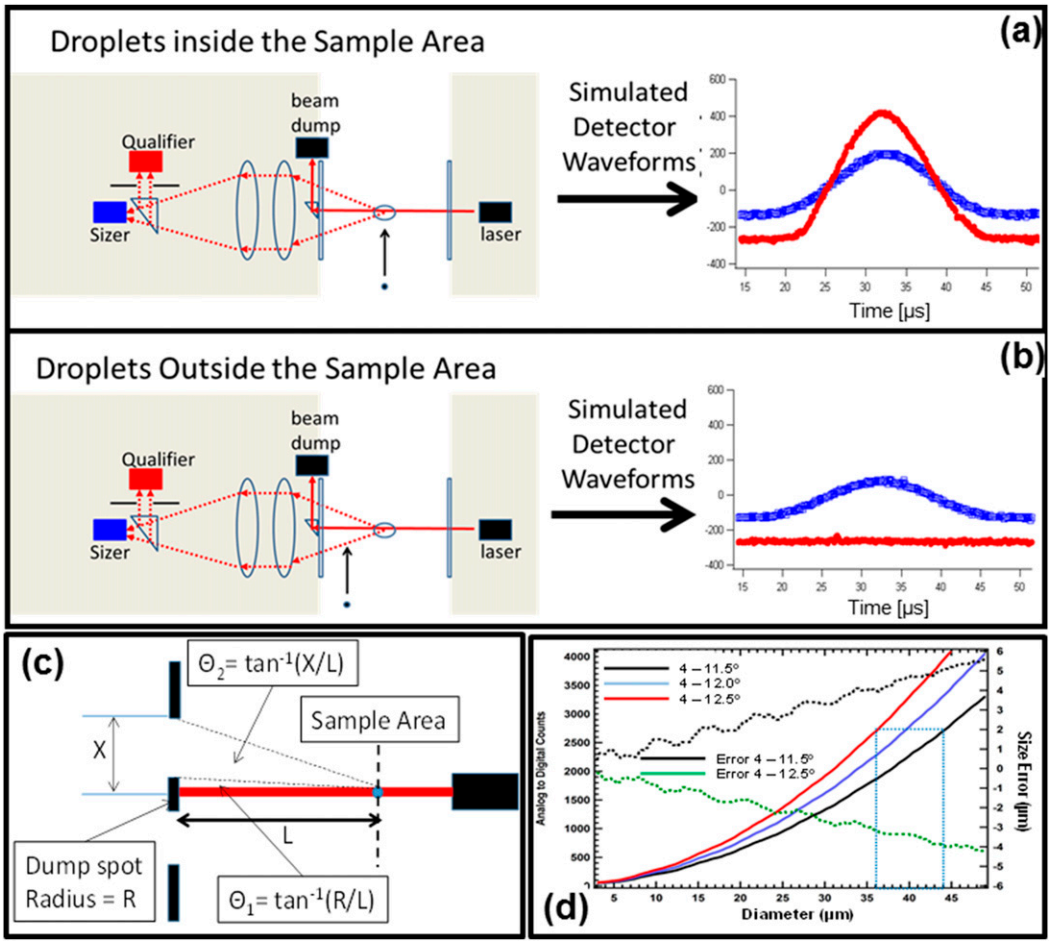

FIG. 9-1. Detection principle of typical scattering probes (FSSP, CDP, FCDP): (a) a particle passes through the laser at the COF, the collected scattered light is recorded by the qualifier and sizer detectors, producing a qualifier signal larger than the sizer, (b) when a particle passes outside the sample area the qualifier (red) is less than the sizer (blue). The collection angles are defined by (c) the optical geometry. (d) The relationship between scattering intensity (solid lines) and collection angle and the sizing error (dashed lines) if the collection angle is different than the nominal 4° to 12°.

Borrmann et al. (2000) modeled the response of an FSSP-300 to ice crystals simulated with rotationally symmetric ellipsoids using T-matrix theory and Meyer (2012) also used T-matrix calculations to evaluate the response of the CAS-POL. Borrmann et al. (2000) concluded that undersizing of ice crystals, based on their maximum dimension, can range from 2 to 5 μm when using ellipsoids with an average aspect ratio of 0.5, whereas the results from Meyer (2012) suggests that the error in sizing is likely less than 20%. More recent modeling of hexagonal ice crystals (Um and McFarquhar 2015), using both the geometric optics method and the Amsterdam discrete dipole approximation, for forward-scattering angles similar to the FSSP and CDP, with aspect ratios (AR) ranging from 0.1 to 4 (Fig. 9-3), show average errors ranging from 13.8% ± 10.9% for AR = 0.5 to 39.6% ± 13.7% for AR = 4.0. As seen in the figure, the derived sizes can be smaller or larger than the maximum geometric diameter, depending on the size range.

(iii) Sizing uncertainties related to particle coincidence

As first discussed by Cooper (1988) and more recently by Cotton et al. (2010), Lance (2012), and Johnson et al. (2014), as the particle number concentration and/or probe sample volume increases so does the probability that more than one particle will be in the sensitive sample volume simultaneously. This can lead to a positive bias in the derived size. The magnitude of this bias has not been quantified numerically or experimentally; however, Cooper (1988) concluded that for the FSSP it was not a significant effect until concentrations

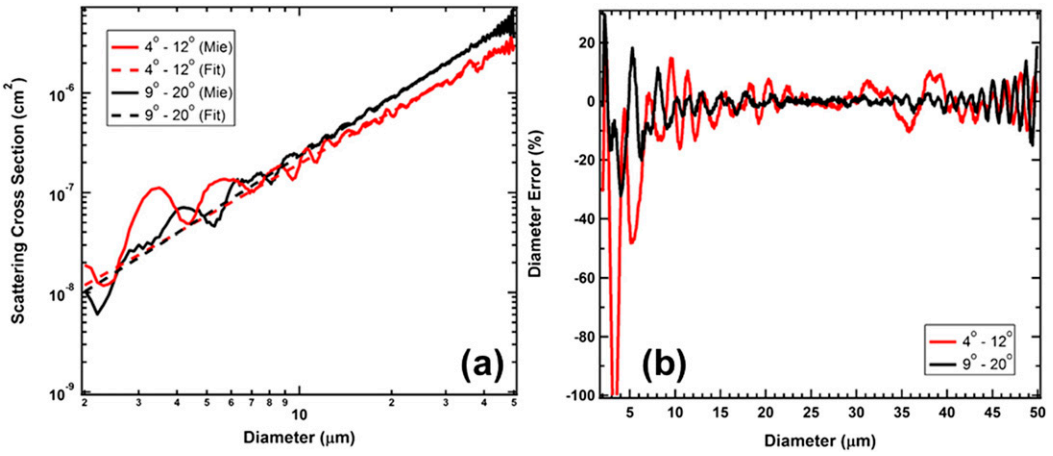

FIG. 9-2. (a) Mie-scattering cross section of water droplets as a function of drop diameter over the solid angles 4°–12° (red) and 9°–20° (black). The dashed lines are power fits to the theoretical cross sections. (b) Estimated error when deriving size from measured scattering.

exceeded 500 cm^{-3}. Observational studies comparing LWC derived from measurements with an unmodified CDP and with a King hot-wire probe [see section 2a(3) below] indicated that the CDP LWC was on average 50% higher than the hot-wire values (Lance 2012). Assuming that most of the error is due to oversizing from coincidence, and that LWC is proportional to the cube of the MVD, a 50% error in LWC is the result of a 25% error in the MVD (using root-sum-squared error propagation).

Cotton et al. (2010) and Johnson et al. (2014) show that multiple droplets in the sample volume of the SID can be erroneously interpreted as ice crystals since their scattering pattern will not be symmetric. In addition, although the trigger volume of the SID is approximately 4 times larger than the OSS, it has an extended sampling volume that is up to 60 times larger, depending on the settings (Cotton et al. 2010) such that if a particle in the extended volume is coincident with one in the trigger volume, the resultant collected light will be interpreted as a single larger particle. Cotton et al. (2010) estimate a 5% probability for 30 cm^{-3}, a concentration that is typical for cirrus but can be much larger in mixed-phase clouds and hence the probability of coincidence will be much higher as well. This would lead to a positive bias toward larger particles. Vochezer et al. (2016) observe the high-resolution scattering patterns from the SID-3 and predict a lower coincidence rate. The difference is that Cotton et al. (2010) and Johnson et al. (2014) use the worst case scenario for coincidence by assuming that after a trigger, a second particle in the extended main-detector sensing volume adds to the scattered image. Vochezer et al. (2016) calculate the coincidence probability assuming the second particle has to be in the much smaller trigger volume.

3) COUNTING LIMITATIONS AND UNCERTAINTIES

As described above, coincidence is the event when more than a single particle is in the detection volume of the instrument. The detection volume is defined as that portion of the beam where light scattered by a particle will produce a signal above the noise threshold and initiate processing by the instrument. The sample volume is that portion of the beam where the scattering signal will be processed to derive size. If two or more particles are in the sample volume, they will be processed as a single particle, and as a result, undercounting occurs. The impact on the FSSP is more serious because of the way that the qualifier is applied (Baumgardner et al. 1985). In the CDP, CAS, and FCDP, the mask on the qualifier optics is used only to accept particles in the DOF when the qualifier signal exceeds the sizing signal. In the FSSP, the mask is designed so that the qualifying detector only sees particles that are outside the DOF, and the particle is rejected if the qualifier signal exceeds that of the sizer. This means that in the case of coincident particles, if the larger one is outside the DOF, it can cause the one in the DOF to be rejected. Hence, coincidence can be a more serious issue with this probe.

The SIDs have a sample area approximately 4 times greater than the OSS, and hence a greater probability of coincidence, although at typical cirrus concentrations (<100 cm^{-3}), this error will be less than 10%. A more serious limitation is the electronic dead time that the SID-2 requires after each particle (50 μs) to process the signals. According to Cotton et al. (2010), the SID-2 can

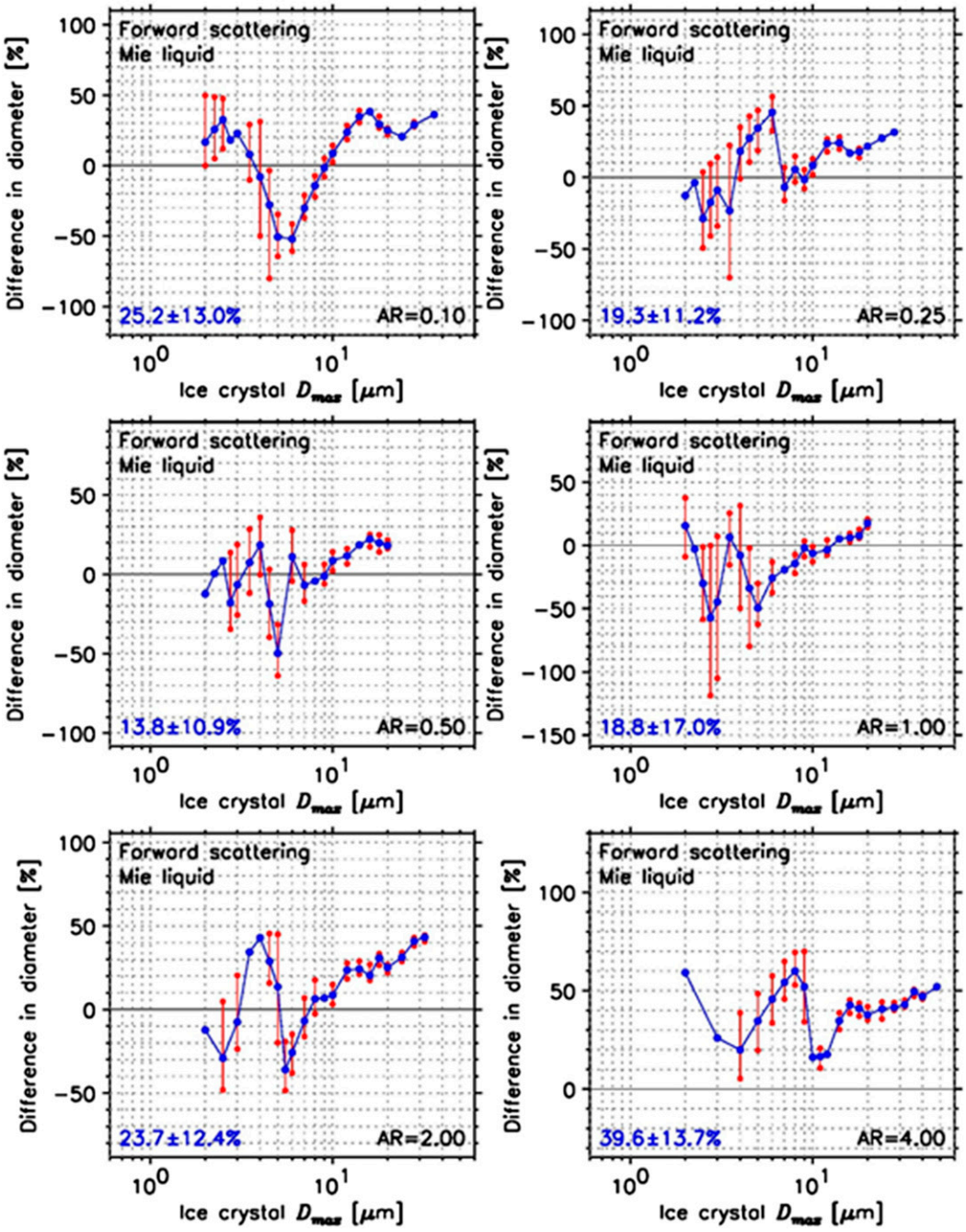

FIG. 9-3. The percent difference between the maximum dimension of hexagonal ice crystals and the dimension that would be derived from Mie scattering is shown as a function of the maximum dimension for different ARs.

process a maximum of 8000 particles each second, which corresponds to about 150 cm^{-3}. Corrections can be applied by estimating the number of particles missed during the dead time (Johnson et al. 2014).

Uncertainties in the sample area contribute to the accuracy with which number and mass concentration is calculated. With the advent of the beam-mapping systems with droplet streams (Lance et al. 2010) this source of uncertainty has been greatly decreased. Note that concentrations of ice crystals are normally small enough that coincidence is not a significant issue; however, in mixed-phase clouds the combined concentrations of water droplets and ice crystals can be large enough that coincidence can have an effect.

Counting uncertainties related to droplet splashing and ice crystal shattering

The tips on the arms of cloud instruments that extend the sample volume forward into the airstream are areas where water droplets and ice crystals impact and disperse into secondary particles, some of which will pass through the sensitive beam and lead to positive biases in the number and mass concentrations, particularly in the smaller size channels dominated by the shattering artifacts (Gardiner and Hallett 1985; Field et al. 2003; Heymsfield 2007; McFarquhar et al. 2007; Baker et al. 2009). The magnitude of this source of measurement error has not been quantified because of the complex nature of shattering that depends on the size of the water droplets and ice crystals, their velocity, the pitch of the aircraft, and the shape of the surface that they impact (Korolev et al. 2013a, b), although some attempt has been made to quantify the number of fragments per ice crystal collision (Vidaurre and Hallett 2009). Although there have been some corrections proposed [discussed in McFarquhar et al. (2017), chapter 11] the major caveat is that measurements made in clouds with ice crystals should be analyzed cautiously.

The optimum alternative is to minimize this source of uncertainty using probe tip designs that direct the particle fragments away from the sensitive volume since the correction algorithms can only offer a partial solution (Korolev and Field 2015). The CDP, FCDP, CPSPD, and some FSSPs have such tips; however, even this solution does not remove all shattered fragments (Korolev et al. 2013a,b) and the interarrival times should still be examined to identify artifacts [discussed in McFarquhar et al. (2017), chapter 11]. Both SID-2 and SID-3 where designed prior to the development of the Korolev style tips and in order to reduce the effect of shattering, the inlet tube of SID-1 was replaced with an open-path design where the placement of the sample volume is well away from the probe laser and detector housing. The probe housing design successfully reduces shattering effects only in cirrus where small ice particles dominate [Cotton et al. (2010) show nonbimodal interarrival time distribution for observations in cirrus].

b. Imaging sensors

The imaging probes that are most frequently employed in aircraft measurements are the Two-Dimensional Cloud and Precipitation spectrometers (2D-C, 2D-P), the Cloud and Precipitation Imaging Probes (CIP, CIP-Gray, and PIP), the Two-Dimensional Stereo spectrometer (2D-S), the High Volume Precipitation Spectrometer (HVPS), and the Cloud Particle Imager (CPI). All of these spectrometers use imaging to reconstruct cloud particle shapes and sizes.

1) MEASUREMENT PRINCIPLES

There are two different types of imaging probes. In the first type the particle image is formed with the help of a linear photodiode array scanned with the frequency proportional to the speed of the particles. The final projected particle image is formed from a sequence of image slices consisting of occulted and blank pixels detected by the photodiode array when the particle was passing through the sample volume. These types of spectrometers are usually referred to as optical array probes (OAPs). Introduced by Knollenberg (1970) the OAP was the first instrument that could make continuous measurements of the size of cloud particles, initially in only a single dimension, then in two dimensions (Knollenberg 1976, 1981). The original 2D design has been improved upon with faster electronics and higher resolution (Baumgardner et al. 2001; Lawson et al. 2006) in the CIP and 2D-S, but the detection technique remains the same.

The second type of imaging probe registers the entire particle image at once on a charge-coupled device (CCD) matrix, when the particle is within the sample volume. This type of spectrometer is represented by the CPI (Lawson et al. 2001), the Holographic Detector for Clouds (HOLODEC; Fugal and Shaw 2009), the Particle Habit Imaging and Polar Scattering probe (PHIPS; Abdelmonem et al. 2011, 2016), and the High Speed Imaging (HSI) probe (Bachalo et al. 2015).

2) OPTOELECTRONIC LIMITATIONS

The optoelectronic limitations of the OAPs have been well documented (Baumgardner and Korolev 1997; Korolev et al. 1991, 1998a; Jensen and Granek 2002; Ulanowski et al. 2004; Connolly et al. 2007; Korolev 2007). The discrete placement of the individual elements in the diode array, and the 50% occultation criterion, introduce a digitization uncertainty of approximately ± 1 size resolution that depends upon where the particle passes across the array. For example, for a probe with 25-μm resolution, drop sizes between 37.5 and 62.5 μm can be registered as 50 μm. The percentage error decreases with particle size.

The nominal DOF is directly proportional to the square of the maximum dimension and the inverse of the incident wavelength. The DOF is in this case defined as that region within which a particle recorded image is within $\pm 10\%$ of the actual particle size (Knollenberg 1970). When the nominal DOF of a particle is less than the distance between the probe's extended arms, there is a large degree of uncertainty in the actual DOF, as well as the particle size. This is because particles outside of the nominal DOF can still form an image

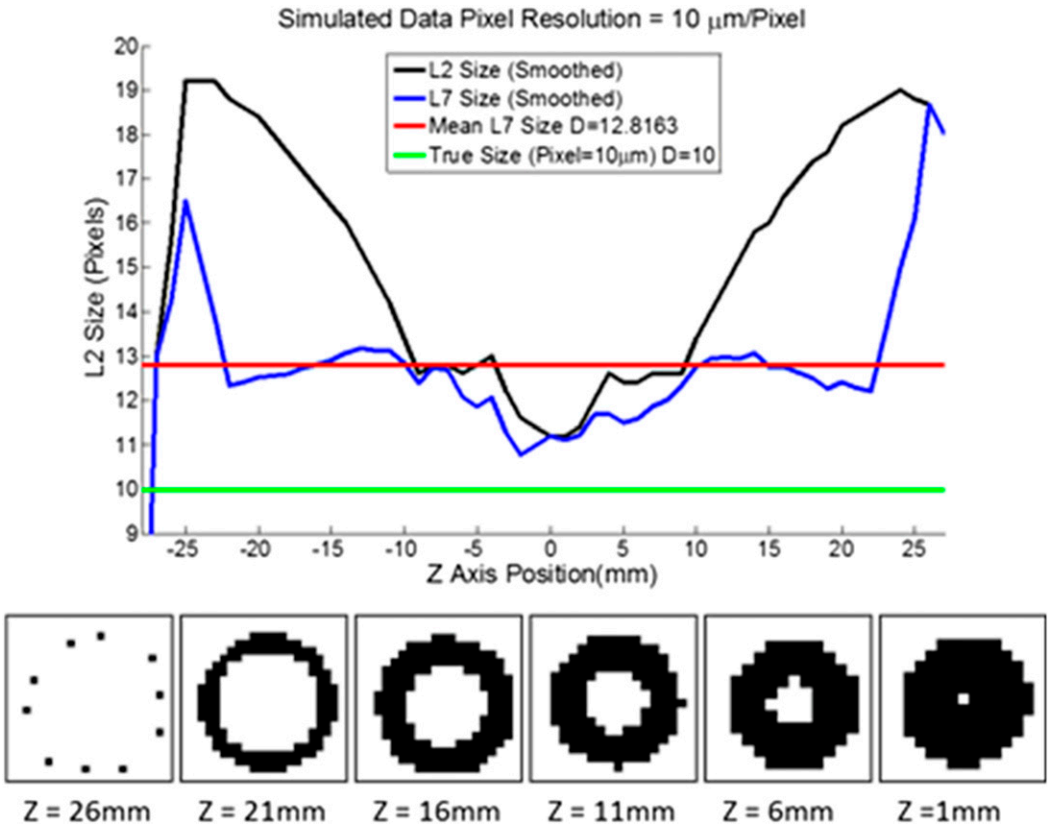

FIG. 9-4. Simulations of the SPEC 2D-S probe showing the image size of a droplet at different distances Z from the COF. The true size is given by the green curve, L2 (black) is the maximum distance across the image, L7 (blue) is the recovered size using the Korolev correction, and the average bias across all the image is given by the red curve.

(Korolev et al. 1998a). As illustrated in Fig. 9-4 for a simulation of the 2D-S, similar to the study by Korolev et al. (1998a), as drops pass farther from the center of focus (COF; $Z = 0$), their recorded image sizes differ from the actual diameter. The line L2 (black) shows the measured size (pixels) of a 10-μm droplet compared to the actual size (red) as a function of distance from the center of focus.

Korolev (2007) derived relationships for spherical water droplets that correct the size of those particles outside the nominal DOF, as well as providing a more accurate DOF to use when calculating sample volume. These relationships, not valid for nonspherical ice crystals, are for water droplets using a 50% occultation level. The curve labeled L7 (blue) in Fig. 9-4 shows the result of applying this correction to the out-of-focus images. Similar corrections have not been derived for ice crystals or for grayscale probes that measure multiple occultation levels for each image. All of the imaging probes use the 50% occultation threshold except the CIP-Gray, which has thresholds of 25%, 50%, and 70%. The higher occultation level could, in principal, better define the DOF and decrease the sizing uncertainty but to date, this has not been evaluated.

An additional issue, especially before the advent of modern, fast-response photodetectors and electronics, is that of undersizing due to the response time of the photodiodes at airspeeds greater than about 80 m s^{-1} (Baumgardner and Korolev 1997). Measurements taken with the 2D-C and early model CIP (pre-2010) require airspeed corrections and their lower size thresholds are limited to approximately 40 μm. Some institutes have upgraded their 2D spectrometers to 10 μm and the CIPs manufactured after 2010 have 15- or 25-μm resolution with gray-level shadowing. The faster response 2D-S has a higher size resolution of 10 μm. The time response of the 2D-S has been validated with laboratory studies up to 220 m s^{-1}, whereas that of the later model CIP has been evaluated up to 150 m s^{-1} with additional studies required to validate the lower size threshold at higher airspeeds.

3) SPLASHING AND SHATTERING

The issue of ice crystal shatter, previously addressed for light-scattering probes, is also a problem with OAPs; however, the much larger sample volumes of the OAPs mean that there is a higher probability that the shattered

fragments will be detected (Korolev and Isaac 2005; Korolev et al. 2011, 2013a; Field et al. 2006; Lawson 2011; Jackson et al. 2014; Korolev and Field 2015). As with the light-scattering probes, there have been some corrections proposed [discussed in McFarquhar et al. (2017), chapter 11]; however, the best alternative is to use probe tip designs that minimize the problem in combination with the correction algorithms since the algorithms only offer a partial solution (Korolev and Field 2015).

4) Data processing uncertainties

There are a number of algorithms that have been developed to minimize uncertainties and account for the limitations that have been discussed for the single-particle spectrometers. Some of these have been generally accepted by the cloud measurement community while others remain under investigation and discussion. These correction procedures are the topic of McFarquhar et al. (2017, chapter 11).

5) Impact of uncertainties on combined sensor measurements

To cover the full size range of cloud ice particles, it is necessary to combine measurements from the single-particle light-scattering and imaging spectrometers. Although these measure with overlapping sizes, matching them is challenging because of their respective uncertainties. Provided the processing is optimized by removing as many artifacts as possible and applying the correction procedures discussed in this chapter and McFarquhar et al. (2017, chapter 11), the agreement can be within the expected accuracy. Figure 9-5 shows a number of examples where a light-scattering spectrometer, the FCDP (red), is compared with an imaging spectrometer, the 2D-S (blue). Examples are taken in an all-liquid cloud, sampled with the Stratton Park Engineering Company (SPEC) Learjet, and an all-ice cloud sampled with the NASA Global Hawk. CPI images are included in each panel of this figure to illustrate the type of cloud particle. The 2D-S minimum detectable particle size is about 10 μm (Lawson et al. 2006). When the FCDP size mode is $<10\,\mu$m there is poorer agreement between the 2D-S and FCDP size distributions. When the FCDP size mode is $>10\,\mu$m the agreement is well within the expected uncertainties in number concentration ($\pm 20\%$) and size (32%). For reference a thick dashed line is drawn at 10 μm on all plots.

The detection efficiency of particles measured by the 2D-S in the 10-μm size bin is less than 100%, and larger particles at the edge of their depth of field may collapse into a single pixel and be erroneously counted in the first bin (Korolev 2007), so statistical corrections are required and counting accuracy is degraded. Shattering and splashing removal is applied (based on interarrival time), and the Korolev correction was applied for out-of-focus water drops in the 2D-S. For the FCDP analysis, shattering removal is applied based on the interarrival times. Coincident particles are rejected based on the symmetry of the particle waveforms as well as transit time rejection based on the size of the particles (assuming a Gaussian beam profile). A depth-of-field threshold is also used to reject particles clipping the edge of the sample volume, but different values are applied for the dense continental clouds and the sparse ice clouds (which requires adjustment of the sample volume).

3. Liquid and ice water detection techniques

LWC and ice water content (IWC), and their sum, the total condensed water content (TWC), are measured using evaporative (heated sensor) and optical (ensemble light scattering) techniques to directly or indirectly derive these quantities.

a. Heated sensors

1) Measurement principles

(i) Hot-wire sensors

The King and Nevzorov probes measure the power required to maintain the sensor at a constant temperature. They are referred to as "first principle" instruments because the heat lost from the sensor due to the transfer of energy via radiation, convection, and evaporation of droplets can be directly calculated based on thermodynamic principles. The energy transfer by radiation is usually ignored because its contribution to the total energy loss is negligible when compared to the other two energy sinks. The King probe (King et al. 1978) was an improvement of its predecessor, the Johnson–William (JW) probe because of how it implemented the measurement of the heat loss by measuring the electrical current required to maintain the sensor at a constant temperature. The LWC is calculated from the residual power derived after subtracting the convective power loss from the total power measured. The convective power can be directly estimated from the measured airspeed and air density, or the average power measured before cloud entry can be used to estimate this convective heat loss. McFarquhar et al. (2017, chapter 11) provides details of how this is done.

The King probe was designed to only measure LWC since ice crystals are not sensed in the same manner as water droplets. The sensor partially responds to ice crystals but not in a predictable manner; hence, data

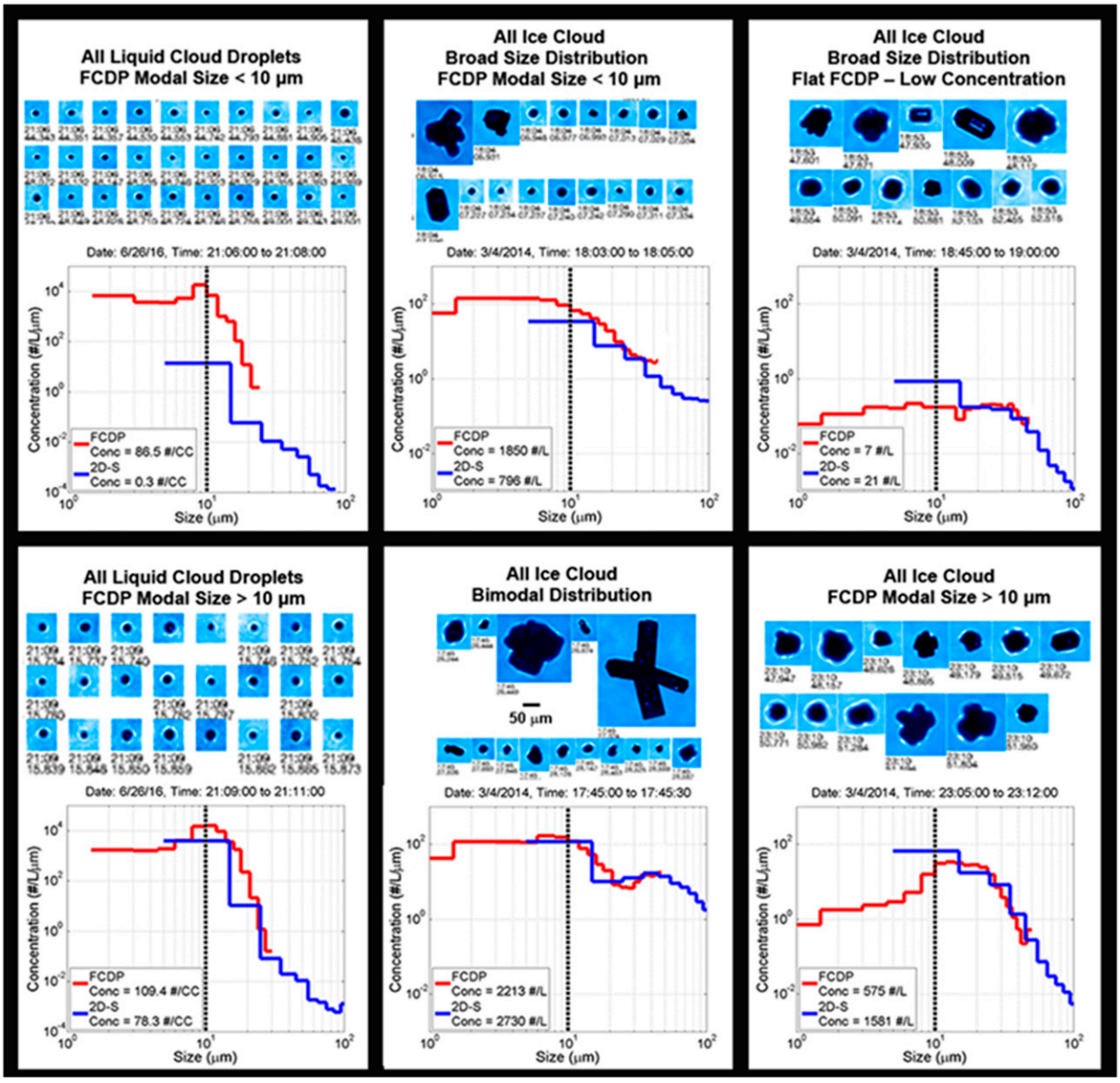

FIG. 9-5. Examples of particle size distributions from the SPEC FCDP (red trace) and 2D-S (blue trace) optical array probe made from the SPEC Learjet in all-liquid clouds and NASA Global Hawk in all-ice cirrus clouds. Example CPI images are shown above each plot. The 2D-S minimum detectable particle size is about 10 μm. When the FCDP size mode is $<10\,\mu$m, there is poorer agreement between the 2D-S and FCDP size distributions. When the FCDP size mode is $>10\,\mu$m, the agreement is good. For reference a thick dashed line is drawn at 10 μm on all plots.

taken with this instrument should be interpreted cautiously in the presence of ice.

The Nevzorov hot-wire probe (Korolev et al. 1998b, 2013b) consists of separate sensors to measure the TWC and the LWC. The TWC sensor consists of a heated cone mounted on a vane, which orients the cone opening directly into the airflow. Like the King probe, the cone is held at a constant temperature sufficient to melt and evaporate the captured liquid and ice particles. The LWC sensor consists of a heated wire wound onto a copper rod that is fixed to the leading edge of the vane. Liquid droplets impacting either sensor should form a thin surface film and evaporate fully. Ice particles, however, tend to break up and fall away from the convex surface of the liquid water sensor, although a residual signal from these ice particles is often observed (Korolev et al. 1998b). As the heated sensors are exposed to the airflow, forced convective cooling due to

the airflow over the sensor adds to the power requirement to melt and evaporate cloud particles. The forced convective cooling depends on the aircraft attitude and environmental conditions. Unlike the King probe, the Nevzorov has a reference sensor, aerodynamically shielded from cloud particles, which partially compensates for this convective cooling and enables the removal of most of the dry-air heat-loss term. The water content, q, can be calculated following

$$q = \frac{P_C - KP_R}{USL^*},$$

where P_C and P_R are the collector and reference sensor power, U is the aircraft true airspeed, S is the sensor sample area, and L^* the energy required to melt and then evaporate the measured hydrometeors. The K parameter is the ratio of the collector to reference power that is dissipated in cloud free air and represents the dry-air heat-loss term. The lack of full compensation of this term by the reference sensor leads to a variation in K during a flight and hence a "baseline drift" of the calculated q. Korolev et al. (1998b) and Abel et al. (2014) show that K is dependent on airspeed and environmental conditions. The probe sensitivity in q can reach $\pm 0.002\,\mathrm{g\,m^{-3}}$, providing that the baseline drift is removed by adequately capturing how K varies over the flight (Abel et al. 2014). The methodology for baseline removal is discussed in McFarquhar et al. (2017, chapter 11).

(ii) Evaporators

The TWC can be derived from measurements of the total water vapor mixing ratio q_t, consisting of the ambient water vapor q_v, plus evaporated cloud particles q_w. Removal of q_v using an independent measurement leaves q_t, which is also the TWC. The q_t is sampled by means of a forward-facing inlet mounted outside the research aircraft and is subsequently measured by closed-cell instruments [e.g., total water probe (TWP), fast in situ stratospheric hygrometer (FISH), closed-path tunable diode laser hygrometer (CLH), and Harvard total water (HTW) isokinetic evaporator; Nicholls et al. 1990; Weinstock et al. 2006; Davis et al. 2007; Schiller et al. 2008; Davidson et al. 2009; Luebke et al. 2013; Krämer et al. 2016]. The gas-phase water q_v is measured simultaneously by either closed-cell instruments connected to a backward-facing inlet or open-path instruments (see references in the studies cited above). The large ice particles are sampled out of an enhanced air volume in comparison to the sampling volume of the gas phase because the large particles cannot follow streamlines around the inlet (Krämer and Afchine 2004; Schiller et al. 2008). The sampling characteristics of the inlets of the different research aircraft have been determined by computational fluid dynamics modeling. As shown in these publications, the aspiration coefficient (or enhancement factor) of the aircraft inlets increases from a minimum value for particles with radii smaller than 300 μm to its maximum value $E_{\max}$, which is the ratio of the flow velocity inside the inlet U_{inlet} and the free flow U_0. IWC is then calculated by using $\mathrm{TWC} = (q_t - q_v)/E_{\max}$.

The counterflow virtual impactor (CVI) derives the TWC by measuring the water vapor mixing ratio after evaporating water droplets and ice crystals (Noone et al. 1988; Ström and Heintzenberg 1994; Twohy et al. 1997, 2003). At the inlet of the CVI, cloud droplets or ice crystals larger than a minimum aerodynamic diameter (5–10 μm, depending on conditions and counterflow) encounter a flow of dry nitrogen gas or air flowing out the tip and are separated from the interstitial aerosol and water vapor. The inertia of the larger hydrometeors overcomes the counterflow stream of gas out the CVI tip while the aerosol particles, as well as some of the smallest droplets and ice crystals, are carried around with the flow. The water vapor that remains after droplet and crystal evaporation is sampled with a hygrometer, downstream of the inlet, to determine the water content. Like the other heated-air techniques, droplets or crystals in a large sampling volume converge into a smaller sample stream within the instrument and concentrations within the CVI are significantly enhanced, which leads to more sensitivity.

2) MEASUREMENT UNCERTAINTIES

There are five primary sources of uncertainty when interpreting measurements from the King and Nevzorov sensors: 1) removal of the convective heat-loss term from the total heat loss measured, 2) sensitivity of the LWC sensors to IWC, 3) collection efficiency, 4) incomplete evaporation of large drops and ice crystals, and 5) bouncing or pooling in the concave elements of the Nevzorov and Water Content Meter (WCM)-2000/3000.

The uncertainty in the convective heat-loss term limits the King probe to a minimum threshold of $0.05\,\mathrm{g\,m^{-3}}$ and accuracy of $\pm 0.05\,\mathrm{g\,m^{-3}}$ (King et al. 1978). The additional reference sensor in the Nevzorov probe decreases the uncertainty to $\pm 0.002\,\mathrm{g\,m^{-3}}$, providing that the baseline drift is adequately removed using the technique described in McFarquhar et al. (2017, chapter 11; Abel et al. 2014). Cober et al. (2001) evaluated the King and Nevzorov sensors in liquid, mixed-phase, and glaciated clouds and concluded that, on average, both the King and Nevzorov LWC sensor responded by as much as 20% to the IWC; however, the response

fluctuated by quite a bit and appeared to be sensitive to airspeed and temperature, as well as the average size of the ice crystals. The collection efficiency for small droplets is an issue for the cylindrical LWC sensors but is more of an issue for the TWC sensor on the Nevzorov probe where high-speed photography has shown that ice crystals can break or bounce out of the sensor cup (Korolev et al. 2013b). A new sensor design has decreased this problem, but comparisons with a CVI indicate that the Nevzorov measurements can still underestimate the TWC, presumably due to incomplete collection of the largest cloud particles. Under conditions of high LWC or large drops, the King probe will also underestimate the LWC (Biter et al. 1987) because of incomplete evaporation of the drops. This is also an issue for both sensors of the Nevzorov probe (Schwarzenboeck et al. 2009; Korolev et al. 2013b).

The current consensus is that ice crystal shattering at the total water forward-facing inlets should not significantly bias the measurements of IWC since most of the shattered ice fragments are probably sampled and evaporated inside of the heated inlet tube. However, this potential source of uncertainty has not received much scrutiny. In addition, although the magnitude has not be quantified, high-speed photography has shown that ice crystals can bounce out of the cup of the Nevzorov and half cylinder of the WCM, and droplet pooling has also been observed (Emery et al. 2004; Korolev et al. 2013b).

One important source of error in the TWC/IWC measurements is the heating of the inlet: in case of insufficient heating to completely evaporate the liquid or ice particles, the measured water vapor concentration is underestimated. Most inlets have a strong bend between the inlet and measurement cell where large ice crystals are shattered into smaller fragments that evaporate much faster than the original ice crystal; however, in case of insufficient heating, the fragments can stick in the bend and build up an ice shell that evaporates only slowly. This can cause a ''memory effect''; that is, the water measurements are enhanced by continuous supplement of water by the ice shell.

The optimum design for a total water instrument is an inlet aspiration response with a high maximum enhancement factor and low cutoff size. A high enhancement factor results in a strong signal from the ice phase in comparison to the gas phase, leading to a broad IWC range with low uncertainty. A low cutoff size minimizes the loss of ice mass. If the cutoff size is too large, then the TWC will be underestimated and a measure of the ice particle size distribution is needed to assess the lost ice mass. Uncertainties in the ice crystal enhancement factor depend on the respective sensor used for measuring the velocity of the flow inside of the inlet tube.

The accuracy of the water measurement is defined by the hygrometer that is operated downstream of the inlet. A survey of a number of hygrometers is given by Meyer et al. (2015). Lower water vapor concentrations in the gas phase and the IWC have higher uncertainties that depend on the sensitivity of the individual hygrometer. The uncertainty also increases with decreasing enhancement factor.

Uncertainty in the CVI TWC measurement is affected by flow and geometry variations related to the enhancement factor of the CVI (estimated uncertainty of 8%), and by calibration, offset, and hysteresis factors related to the hygrometer (estimated at 5%, 10%, and 5%, respectively). Propagating the error with root sum square (RSS) leads to an overall uncertainty in TWC of approximately 15%.

The probes that measure bulk TWC are known to saturate at high TWCs and airspeeds. Thus, an isokinetic evaporator probe (IKP) and a subsequently redesigned version (IKP2) have been developed to measure TWCs up to $10\,g\,m^{-3}$ at $200\,m\,s^{-1}$ airspeeds (Davison et al. 2009, 2011). The isokinetic flow through a 7-mm-diameter inlet provides a near unity collection efficiency for both cloud particles and water vapor; after evaporation, the TWC is estimated by subtracting the ambient vapor measured by another probe.

A potential source of uncertainty is in the desynchronization of background humidity measurements with that measured by the evaporator due to a different length of sampling lines, which may significantly contribute in the uncertainty of TWC measurements (A. Korolev 2016, personal communication). This is specifically relevant to the turbulent environment and warmer temperatures ($T > -10°C$).

b. *Optical sensors*

1) MEASUREMENT PRINCIPLES

The Particle Volume Monitor (PVM) model 100A is closely related to a class of instruments termed ''laser-diffraction particle-sizing instruments.'' The PVM uses a collimated laser to irradiate an ensemble of particles that scatter light onto a large-area photo diode in front of which is placed a fixed spatial filter with varying radial transmissions that converts the scattered light to a measure of the integrated particle volume concentration C_v. (Gerber et al. 1994). The PVM has been used primarily to measure C_v in warm water clouds; however, IWC measurements made in wave clouds where the ice crystals were small (effective radius $< 10\,\mu m$) and quasi-spherical were compared with those from a CVI and showed better than 20% agreement between the two instruments (Gerber et al. 1998). In mixed-phase clouds, however, IWC in the PVM cannot be differentiated from LWC.

2) MEASUREMENT UNCERTAINTIES

The PVM begins to lose its response to droplets larger than 30 μm (Gerber et al. 1994; Wendisch et al. 2002) and presumably to ice crystals larger than this size, as well. Given that there have been no quantitative studies of the response of the PVM to larger sizes of ice crystals than 20 μm, or that were not quasi-spherical in shape, the uncertainty in derived IWC/TWC is unknown at this time. As with the King probe, interpretations of the PVM measurements should be made with great caution in mixed-phase or glaciated clouds.

4. Shape measurements

Differentiating water droplets from ice crystals in mixed-phased clouds and extracting shape information from ice crystals is a major challenge with far reaching scientific ramifications. There is growing evidence, most of it indirect or from remote sensing, that atmospheric ice crystals tend to have shapes departing from idealized geometries based on smooth, hexagonal prisms [for a review see Heymsfield et al. (2017, chapter 2)]. It is important in this context that roughness can dramatically alter the scattering properties of ice crystals. For example, it can significantly reduce the scattering asymmetry parameter, thus shifting radiative forcing toward negative values [Ulanowski et al. 2006; Yang and Liou 1998; Yang et al. 2013; Schnaiter et al. 2016; see also references in Heymsfield et al. (2017, chapter 2)]. Hence it is important to quantify the fine detail of ice crystal geometry.

The differentiation of droplets and ice crystals from imaging probe measurements largely depends on the complexity of the ice crystal. In some cases, only six or more pixels are required to identify drizzle drops (Korolev and Sussman 2000; Cober et al. 2001); however, Korolev and Sussman (2000) conclude a minimum of 12–14 pixels are needed to even identify a hexagonal plate. McFarquhar et al. (2013) distinguished quasi-spherical ice crystals from water droplets in CPI images acquired in Arctic mixed-phase clouds, Lawson et al. (2015) used CPI images to distinguish water droplets from ice particles in the size range of 30 to 500 μm in mixed-phase tropical cumulus clouds, and more recent field measurements in tropical tropopause layer (TTL) cirrus during the Airborne Tropical Tropopause Experiment (ATTREX) campaign with the CPI (S. Woods 2016, personal communication) show that ice crystals as small as 50 μm can be distinguished by ice habit into quasi-spheroids, columns, plates, rosettes, budding rosettes, and irregulars; however, frozen droplets that have retained their sphericity cannot be distinguished from liquid drops (Korolev and Sussman 2000) regardless of their size.

The optical resolution limitations of imaging probes manifest themselves most strongly for smaller particles (Korolev et al. 1998a; Korolev 2007; Ulanowski et al. 2004; Connolly et al. 2007). It is possible to bypass them by obtaining light-scattering ''patterns'' instead of images. Such patterns can be acquired from relatively large sample volumes, as there is no sharply defined image plane to limit resolution. Successive models of the SID obtain scattering patterns with progressively higher angular resolution, up to imaging array level. The earlier designs rely on multielement detectors measuring mainly the azimuthal scattering, allowing the discrimination between droplets and ice crystals, as well as some degree of ice shape characterization (Hirst et al. 2001; Cotton et al. 2010, 2013; Johnson et al. 2014). The later ones, collectively known as SID-3, acquire high-resolution 2D scattering patterns (Kaye et al. 2008; Ulanowski and Schnaiter 2011; Ulanowski et al. 2012, 2014). 2D scattering patterns offer high potential for detailed shape characterization (Clarke et al. 2006; Kaye et al. 2008; Schnaiter et al. 2016). Ice particle roughness can also be obtained due to the presence of multiple interfering waves giving rise to speckle (Ulanowski et al. 2006, 2012). SID-3 measurements indicated that the majority of ice particles in midlatitude clouds were rough or had complex structure (Ulanowski et al. 2014). Figure 9-6 shows measurements with the SID-3 of test particles of increasing complexity and/or roughness, illustrating rising amount of speckle. Moreover, the speckle permits essentially calibration-free sizing (Ulanowski et al. 2012).

Polarimetric spectrometers measure the change in polarization state of light scattered by individual particles (Glen and Brooks 2013; Baumgardner et al. 2014). Figure 9-7 illustrates airborne measurements made with a CAS-POL on the U.K. British Aerospace 146 (BAe-146) aircraft in all liquid water, all ice, and all volcanic ash clouds. The three different types of particles are differentiated by comparing the forward scattered light with the polarized backscattered components. The polarization measurements, although potentially able to provide more detailed information on the morphology of small ice crystals, need much more detailed studies in the laboratory and cloud chambers to determine the thresholds separating water droplets from ice crystals as a function of size and shape complexity.

5. Direct measurement of cloud particle optical properties

The optical properties of ice particles—such as extinction coefficient B_{ext}, asymmetry factor g, and

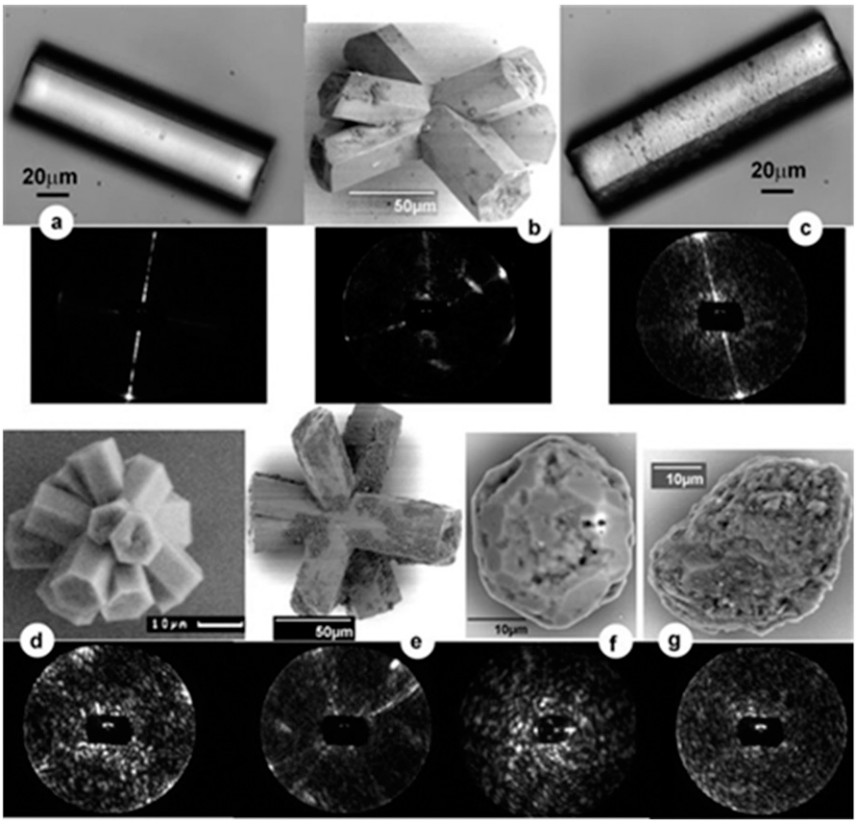

FIG. 9-6. (top) Images of ice analog and mineral dust test particles from optical microscopy [(a),(c) ice analog columns] or scanning electron microscope (SEM), with size scales shown in insets. (bottom) Corresponding SID-3 scattering patterns [adapted from Ulanowski et al. (2014)].

scattering phase function P_θ—impact how clouds interact with solar and terrestrial radiation and modulate climate change. These properties can be derived from the size and shape measurements made by optical spectrometers, but a great deal of uncertainty is involved with this approach because of the insufficient information on the morphological structure of the ice, the imprecise nature of the models, and the unresolved surface characteristics. Four instruments, illustrated in Fig. 9-8, were developed specifically to measure some of these optical properties: the Polar Nephelometer (PN), Cloud Integrating Nephelometer (CIN), Cloud Extinction Probe (CEP), and the PHIPS on board the German High Altitude and Long Range Research Aircraft (HALO) (PHIPS-HALO).

The PN (Fig. 9-8a) measures the phase function from an ensemble of particles (Gayet et al. 1997) using a circular array of photo diodes to detect light scattered from ±3.5° to ±169° at a wavelength of 804 nm. The derivation of B_{ext} and g requires the integration of the scattered light over the scattering angles from 0° to 180°.

The CIN directly estimates g and B_{ext} at a wavelength of 635 nm (Gerber et al. 2000). A collimated laser-diode beam illuminates cloud particles that pass through the probe's aperture (Fig. 9-8b). These particles scatter light that is collected by a set of four Lambertian sensors over an angle range of 10°–175°.

The CEP derives B_{ext} directly using the transmissiometric method for the measurement of the attenuation of light between the receiver and transmitter (Fig. 9-8c). The advantages of this approach are: B_{ext} is derived from first principles, the sample volume is quite large, and there is minimal impact from ice shattering because of the large spatial separation (up to 10 m or higher) between the transmitter and receiver (Wendisch and Brenguier 2013).

The PHIPS-HALO, shown schematically in Fig. 9-8d, combines stereo imaging of individual cloud particles with simultaneous measurement of the polar scattering function of the same particle from 0° to 170° (Abdelmonem et al. 2011, 2016).

There are two primary sources of uncertainty in the derivation of g and B_{ext}. The PN, CN, and PHIPS-HALO do not integrate the light scattering over the complete angular range from 0° to 180° that is needed to derive B_{ext}, although PHIPS-HALO only misses the

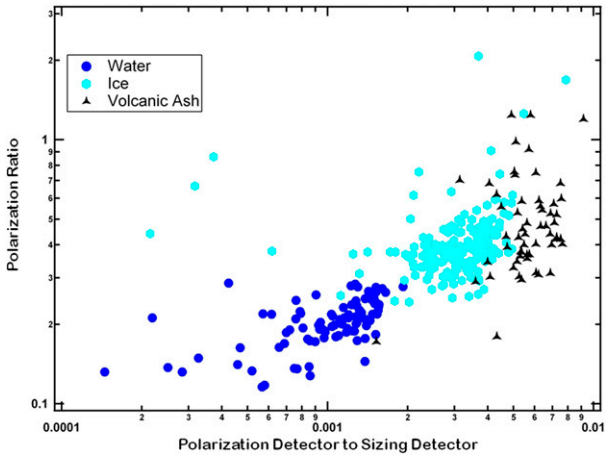

FIG. 9-7. The colored markers indicate in which regions of water droplet (dark blue), ice crystal (light blue), or ash (black) measurements were made (figure courtesy of J. Dorsey, University of Manchester).

fraction from 170° to 180°. This leads to the PN underestimating B_{ext} by 20%–30% and the CIN by >50%. These fractions are rather larger because ice crystals larger than the wavelength of the laser light scatter a large fraction of the incident light in the near-forward direction as a result of diffraction. Corrections for the undetected light have been derived for the PN (Gayet et al. 2002) and the CIN (Gerber et al. 2000), and the estimated uncertainties in B_{ext} are 25% and 15%, respectively.

Ice crystal shattering on the PN, CIN, and PHIPS-HALO is the second source of measurement uncertainty. The magnitude of this error has not been quantified but is potentially the source of a large positive bias in the measurements if ice crystals larger than approximately 100 μm are encountered. As with all instruments with protruding inlets, caution is recommended when interpreting the measurements when shattering is a possibility.

6. Uncertainties related to sampling statistics and instrument location

Under the assumption of Poisson statistics, that is that cloud particles are randomly distributed in space, the probability that a sample represents the parent population is $1 - n^{-1/2}$, where n is the number of particles detected. For example, if 100 droplets are measured, there is 90% probability that these are representative of the parent population. Following Hallett (2003), Fig. 9-9 illustrates this issue for six different spectrometers by calculating the distance that an aircraft would need to travel in order to sample 100 particles at a concentration of 10 L^{-1}, a typical concentration of cirrus crystals. Two methods are used to calculate the sample areas of the OAPs [see McFarquhar et al. (2017, chapter 11) for more details], "All-In" (solid lines) and "Center-In." Although Center-In provides the larger sample area, it is usually applied only to circular or quasi-circular images as there is greater uncertainty when implementing it for nonspherical ice crystals.

The impact of sampling statistics on cirrus climatology can also be seen in Fig. 9-10 taken from Krämer et al. (2016) showing the absence of low concentrations of small crystals in the measurements (within the black box) when compared with modeling results that otherwise compare well with the measurements. As seen in Fig. 9-9, more than a kilometer of cloud is needed to get a statistically representative sample for crystals smaller than 40-μm diameter, suggesting that the smaller crystals are being undersampled with the current instruments. The data are a compilation of measurements taken during many field campaigns with FSSPs, CDPs, CASs, CIPs, and 2D-Ss.

Impact of mounting location

The mounting location on an aircraft is critical for those cloud instruments that need to measure particle properties that are not influenced by airflow distortion caused by the fuselage or wings. This issue has been the topic of a number of workshops (Baumgardner and Huebert 1993; Wendisch et al. 2004) that highlighted how size distributions are biased because of the presence of shadow zones or the convergence/divergence of streamlines that inertially separate cloud particles. Both observational (e.g., King et al. 1984; Twohy and Rogers 1993) and theoretical (e.g., King 1984; Norment 1985, 1988) studies have shown that there are shadow zones where no particles will be measured and other regions on the aircraft where there are size-dependent biases. In addition, the instruments themselves present blockage of the flow that changes the local airspeed so that the particle trajectories may also be altered. Finally, not only does flow distortion possibly cause size sorting but King (1984) showed that differential shear led to preferential rotation of ice crystals so that images from OAPs would sometimes be incorrectly interpreted, for example, platelike crystals were rotated in the flow so that they were viewed edge on and interpreted as columns. Some probes like the 2D-S or 3V-CPI may be less susceptible to orientation of crystals because of their multiple views; however, caution must be used when mounting these instruments as well as interpreting the data since they are particularly sensitive to angle attack and sideslip angles because of the inlets.

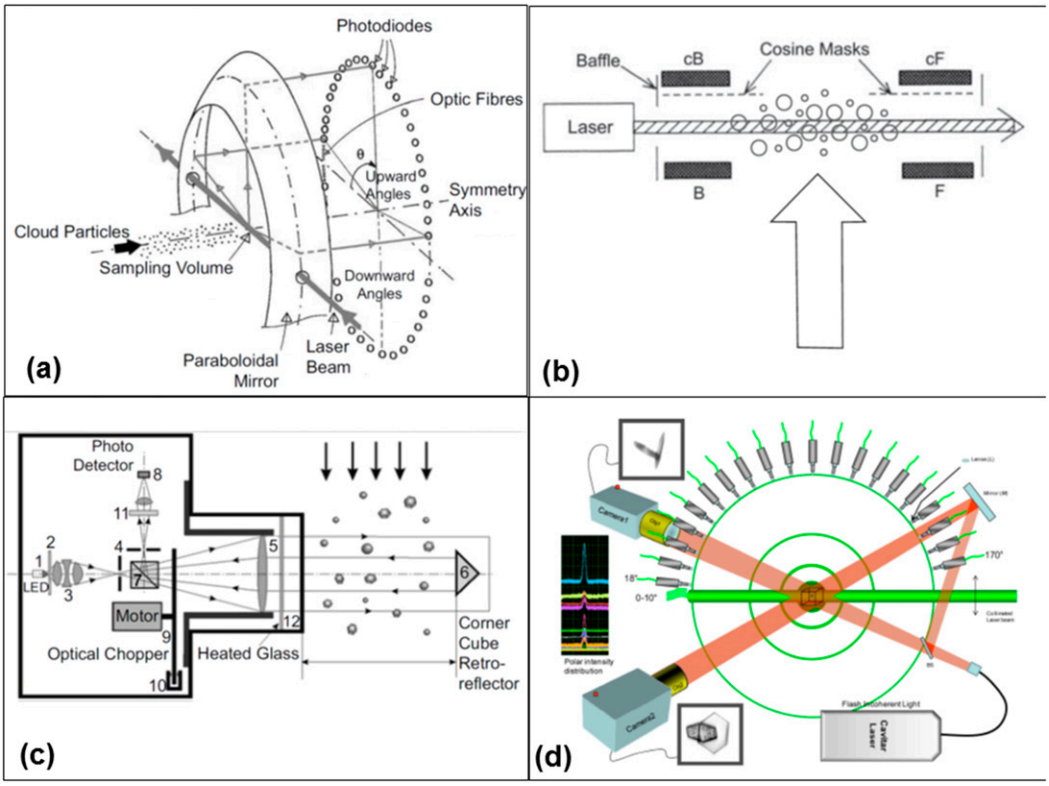

FIG. 9-8. Four instruments that measure optical properties of ice crystals: (a) PN, which measures phase function; (b) CIN; (c) CEP; and (d) PHIPS-HALO.

In summary, although most research aircraft have been evaluated for optimum placement of instruments, the data analyst must be aware of potential airflow issues when analyzing datasets.

7. Additional instruments

We have discussed the uncertainties and limitations of the instruments that are most widely deployed for measuring ice in clouds; however, to close this chapter, it is worth a brief discussion of integrated measuring systems that offer advantages with respect to collocated measurements and to introduce new instruments that are just becoming available but have not been vetted to the same level of scrutiny as the ones that have been discussed earlier.

a. Hybrid sensors

Hybrid instruments are those that combine multiple sensors in a single package. The Cloud, Aerosol and Precipitation Spectrometer (CAPS) integrates a CAS, CIP, King probe along with airspeed, temperature and humidity sensor. The Cloud Combination Probe (CCP) is the same as the CAPS but replaces the CAS with a CDP. The Hawkeye and 3V-CPI also combine sensors, a 2D-S, FCDP, and CPI in the former and a 2D-S and CPI in the latter. Further, the PHIPS-HALO (Schön et al. 2011; Ulanowski and Schnaiter 2011; Abdelmonem et al. 2011, 2016) combines a stereoscopic imager with a polar nephelometer and has a very well-defined sample volume, a major advantage over other imaging spectrometers.

Packaging multiple sensors not only saves space by requiring only a single mounting point on the aircraft, but with nearly collocated sample volumes it is easier to merge overlapping size distributions from cloud and precipitation spectrometers when sampling spatially inhomogeneous cloud properties. Another advantage with the Hawkeye and 3V-CPI is that the 2D-S portion can be set to trigger the CPI on particles larger than a selected size (cut size). This is useful in mixed-phase cloud when detecting the onset of ice with the CPI in clouds with a high concentration of small cloud drops that would otherwise dominate the CPI bandwidth. The 3V-CPI also provides three views of the same particle, albeit with a small sample volume (Fig. 9-11), but this is still very useful in some cloud regimes. Finally, the mechanical stability using a tube instead of arms makes the

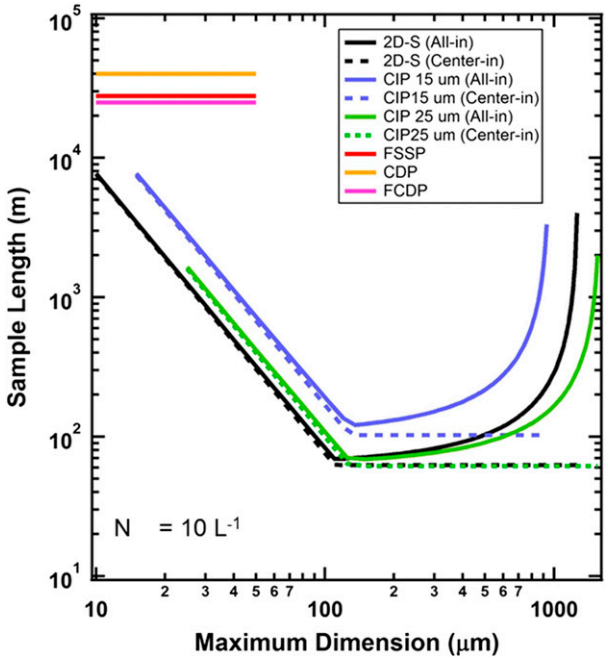

FIG. 9-9. The number of meters needed to sample 100 particles when the crystal concentration is 10 L^{-1} is shown as a function of particle diameter for six spectrometers: 2D-S (black), 15 μm CIP (blue), 25 μm CIP (green), FSSP (red), CDP (orange), and FCDP (magenta) using two methods of determining the sample areas, All-In (solid) and Center-In (dashed).

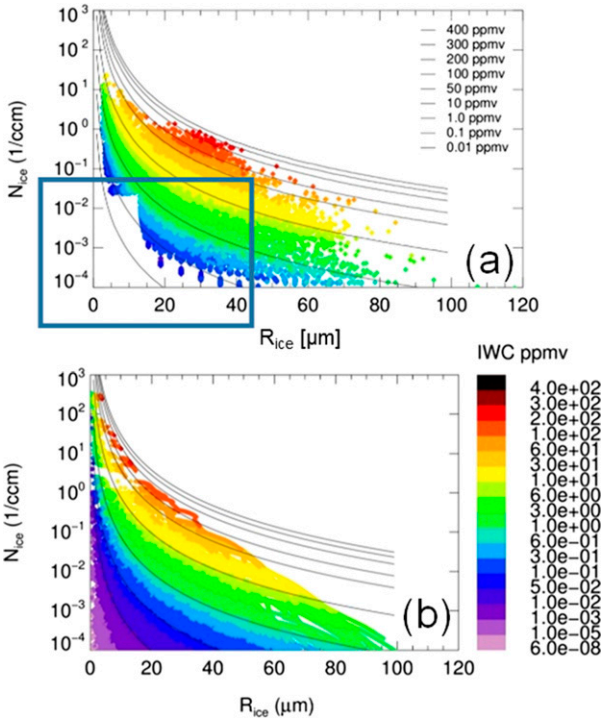

FIG. 9-10. The (a) measured (blue box highlights possible undersampling of small crystals) and (b) modeled ice crystal concentrations are shown as a function of radius. The color coding denotes the ice water content that was measured independently [taken from Krämer et al. (2016)].

task of identifying 2D-S stereo images much more reliable; however, the disadvantage is that there is a higher probability of crystal shattering with the subsequent need to process carefully for artifacts.

One potential issue that arises with those hybrid systems that use a single inlet to direct the particle stream to the probe sample is the enhanced probability of crystal breakup on the leading edge of the inlet. Some correction can be done using interarrival time detection but care should be taken when interpreting the measurements.

b. Next-generation sensors

There are a number of newer instruments that have the potential for providing more extensive information because of their unique measurement capabilities. The HOLODEC (Fugal and Shaw 2009) and the PHIPS-HALO (already discussed) are currently the furthest along in their development with the most flight hours. Both require extensive postprocessing but provide high-resolution, detailed information that resolves droplets from ice as well as providing detail on morphological characteristics. Another advantage offered by holographic techniques is the ability to reject particles, during the analysis, that are close to the probe arms, and deemed to be potentially affected by shattering artifacts. The additional information from the PHIPS-HALO of phase function coupled with the image of the particle promises to open a new avenue of research into the optical properties of clouds. The HSI (Bachalo et al. 2015) is an imaging probe with much better definition of sample volume than possible with the current OAPS. The Airborne Laser Interferometric Drop Sizer (ALIDS; Porcheron et al. 2015) is a technique that is advertised as having a much larger sample volume then the current light-scattering probes and better defined volume than the OAPS. Although the laboratory results seem promising, it has not been tested on an airborne platform.

8. Summary

The basic measurement principles, limitations, and uncertainties have been described for the most frequently deployed, airborne instruments for in situ measurements of the size and number concentrations of cloud particles as well as their liquid and ice water concentrations. The motive for this chapter is mainly to educate users who may not be experts in cloud measurements but need them for analyzing cloud properties,

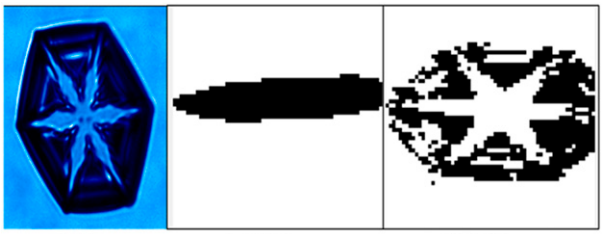

FIG. 9-11. An example of a large hexagonal ice crystal imaged by the 3V-CPI instrument. In this example, the CPI and vertical channel of the 2D-S image the basal plane of the crystal, while the horizontal channel of the 2D-S images the edge of the same particle. Based on these different views of the particle, the horizontal 2D-S channel would underestimate the particle mass by more than factor of 2.

evaluating remote sensing algorithms, and developing parameterizations for cloud and climate models. It is clear no single instrument can provide a complete characterization of cloud properties, and every instrument has issues that limit the accuracy of the measurement. If cognizant of the known caveats associated with each sensor, the data user can factor them in when analyzing the measurements, successfully avoiding publishing results that may, at best be questionable, and at worst lead others down a wrong scientific path.

From the material presented above, we can conclude the following:

- There are no LWC/TWC instruments that can completely separate LWC from IWC.
- Droplets and ice crystals larger than approximately 100–200 μm can be differentiated with OAPS, the CPI can do so down to 35 μm and below this size the SIDs, CAS-POL, and CPSPD show promise but a great deal more effort is needed to characterize their measurements.
- Droplets and ice crystals larger than 100–200 μm, measured with OAPS, can be sized to $\pm$20%, and concentrations better than $\pm$50% with appropriate corrections made to remove artifacts. The derivation of size and concentration below 100 μm is uncertain to approximately $\pm$50% and $\pm$100%, respectively, with increasing uncertainty as the particle size decreases. These uncertainties do not take into account the contributions from ice crystal shattering.
- The uncertainty in sizing and concentration measurements by the light-scattering spectrometers, in the absence of shattering, is a maximum of respectively $\pm$50% and $\pm$20%.
- All processes that require knowledge of the phase and concentration of particles smaller than 100 μm remain poorly understood because of the measurement limitations. These include primary and secondary ice production and also impact assumptions needed for remote sensing retrievals.

There is clearly the need for improvements in measurement capabilities, as well as better understanding how our knowledge of ice formation and evolution may be impacted by the lack of more accurate measurements. Some of the recommended steps that could be taken to contribute to improvements are as follows:

- An in-depth evaluation of the grayscale imaging to determine if utilization of the feature can better define image probe sample volume.
- Extensive laboratory and cloud chamber evaluations of the polarimetric technique to relate changes in polarization state to particle morphology.
- Additional studies to determine if the sample area of scattering probes is sensitive to particle size.
- Improvement of probe designs to minimize or avoid shattering.
- Better placement of probes to reduce interference from airflow around aircraft structures.
- In-depth evaluation of how measurement uncertainties and limitations impact our understanding of cloud processes in general, and ice formation and evolution in particular.
- Detailed modeling of the optical response of the probes to particles of different sizes and shapes and how the different probes respond to them.
- In addition to gross particle shape, fine detail and roughness should be quantified, as they strongly influence radiative properties.

And finally, how can we determine what accuracy is needed to fill remaining gaps in understanding of ice formation and evolution in clouds? Are the current suite of instruments sufficient and we only need more extensive measurements, or are we truly missing important microphysical processes because of measurement limitations and uncertainties?

Acknowledgments. The authors thank the two anonymous reviewers who offered detailed comments and suggestions that significantly clarified and improved the content of this chapter. Funding for this chapter was partially provided by the International Commission on Clouds and Precipitation and by Droplet Measurement Technologies. The authors would like to thank the many sponsors who have provided funding for the monograph: Leibniz Institute for Tropospheric Research (TROPOS), Forschungszentrum Jülich (FZJ), and Deutsches Zentrum für Luft- und Raumfahrt (DLR), Germany; ETH Zurich, Switzerland; National Center

for Atmospheric Research (NCAR), United States; the Met Office, United Kingdom; the University of Illinois, United States; Environment and Climate Change Canada (ECCC), Canada; National Science Foundation (NSF), AGS 1723548, National Aeronautics and Space Administration (NASA), United States; the International Commission on Clouds and Precipitation (ICCP), the European Facility for Airborne Research (EUFAR), and Droplet Measurement Technologies (DMT), United States. NCAR is sponsored by the NSF. Any opinions, findings, and conclusions or recommendations expressed in this publication are those of the author(s) and do not necessarily reflect the views of the National Science Foundation.

REFERENCES

Abel, S. J., R. J Cotton, P. A. Barrett, and A. K. Vance, 2014: A comparison of ice water content measurement techniques on the FAAM BAe-146 aircraft. *Atmos. Meas. Tech.*, **7**, 3007–3022, doi:10.5194/amt-7-3007-2014.

Abdelmonem, A., M. Schnaiter, P. Amsler, E. Hesse, J. Meyer, and T. Leisner, 2011: First correlated measurements of the shape and light scattering properties of cloud particles using the novel Particle Habit Imaging and Polar Scattering (PHIPS) probe. *Atmos. Meas. Tech.*, **4**, 2125–2142, doi:10.5194/amt-4-2125-2011.

——, E. Järvinen, D. Duft, E. Hirst, S. Vogt, T. Leisner, and M. Schnaiter, 2016: PHIPS–HALO: The airborne Particle Habit Imaging and Polar Scattering probe. Part I: Design and operation. *Atmos. Meas. Tech.*, **9**, 3131–3144, doi:10.5194/amt-9-3131-2016.

Bachalo, W. D., 1980: A method for measuring the size and velocity of spheres by dual beam light scatter interferometry. *Appl. Opt.*, **19**, 363–370, doi:10.1364/AO.19.000363.

——, J. W. Strapp, E. Biagio, A. Korolev, and M. Wolde, 2015: Performance of the newly developed High Speed Imaging (HSI) probe for measurements of size and concentration of ice crystals and identification of phase composition of clouds. *Extended Abstracts, SAE 2015 Int. Conf. on Icing of Aircraft, Engines, and Structures*, Prague, Czech Republic, SAE, 1–4.

Baker, B., Q. Mo, R. P. Lawson, D. O'Connor, and A. Korolev, 2009: The effects of precipitation on cloud droplet measurement devices. *J. Atmos. Oceanic Technol.*, **26**, 1404–1409, doi:10.1175/2009JTECHA1191.1.

Baumgardner, D., and B. Huebert, 1993: The airborne aerosol inlet workshop: Meeting report. *J. Aerosol Sci.*, **24**, 835–846, doi:10.1016/0021-8502(93)90050-J.

——, and A. Korolev, 1997: Airspeed corrections for optical array probe sample volumes. *J. Atmos. Oceanic Technol.*, **14**, 1224–1229, doi:10.1175/1520-0426(1997)014<1224:ACFOAP>2.0.CO;2.

——, J. W. Strapp, and J. E. Dye, 1985: Evaluation of the forward scattering spectrometer probe. Part II: Corrections for coincidence and dead-time losses. *J. Atmos. Oceanic Technol.*, **2**, 626–632, doi:10.1175/1520-0426(1985)002<0626:EOTFSS>2.0.CO;2.

——, H. Jonsson, W. Dawson, D. O'Connor, and R. Newton, 2001: The cloud, aerosol and precipitation spectrometer (CAPS): A new instrument for cloud investigations. *Atmos. Res.*, **59–60**, 251–264, doi:10.1016/S0169-8095(01)00119-3.

——, and Coauthors, 2011a: Airborne instruments to measure atmospheric aerosol particles, clouds and radiation: A cook's tour of mature and emerging technology. *Atmos. Res.*, **101**, 10–29, doi:10.1016/j.atmosres.2011.06.021.

——, and Coauthors, 2011b: In situ, airborne instrumentation: Addressing and solving measurement problems in ice clouds. *Bull. Amer. Meteor. Soc.*, **93**, 29–34, doi:10.1175/BAMS-D-11-00123.1.

——, R. Newton, M. Krämer, J. Meyer, A. Beyer, M. Wendisch, and P. Vochezer, 2014: The Cloud Particle Spectrometer with Polarization Detection (CPSPD): A next generation open-path cloud probe for distinguishing liquid cloud droplets from ice crystals. *Atmos. Res.*, **142**, 2–14, doi:10.1016/j.atmosres.2013.12.010.

Beswick, K., D. Baumgardner, M. Gallagher, A. Volz-Thomas, P. Nedelec, K. Y. Wang, and S. Lance, 2014: The backscatter cloud probe—A compact low-profile autonomous optical spectrometer. *Atmos. Meas. Tech.*, **7**, 1443–1457, doi:10.5194/amt-7-1443-2014.

Biter, C. J., J. E. Dye, D. Huffman, and W. D. King, 1987: The drop response of the CSIRO liquid water content. *J. Atmos. Oceanic Technol.*, **4**, 359–367, doi:10.1175/1520-0426(1987)004<0359:TDSROT>2.0.CO;2.

Borrmann, S., L. Beiping, and M. Mishchenko, 2000: Application of the T-matrix method to the measurement of aspherical (ellipsoidal) particles with forward scattering optical particle counters. *J. Aerosol Sci.*, **31**, 789–799, doi:10.1016/S0021-8502(99)00563-7.

Clarke, A. J. M., E. Hesse, Z. Ulanowski, and P. H. Kaye, 2006: A 3D implementation of ray tracing combined with diffraction on facets. *J. Quant. Spectrosc. Radiat. Transfer*, **100**, 103–114, doi:10.1016/j.jqsrt.2005.11.028.

Cober, S., G. A. Isaacs, A. V. Korolev, and W. J. Strapp, 2001: Assessing cloud phase conditions. *J. Appl. Meteor.*, **40**, 1967–1983, doi:10.1175/1520-0450(2001)040<1967:ACPC>2.0.CO;2.

Connolly, P. J., M. J. Flynn, Z. Ulanowski, T. W. Choularton, M. W. Gallagher, and K. N. Bower, 2007: Calibration of 2-D imaging probes using calibration beads and ice crystal analogues. *J. Atmos. Oceanic Technol.*, **24**, 1860–1879, doi:10.1175/JTECH2096.1.

Cooper, W. A., 1988: Effects of coincidence on measurements with a forward scattering spectrometer probe. *J. Atmos. Oceanic Technol.*, **5**, 823–832, doi:10.1175/1520-0426(1988)005<0823:EOCOMW>2.0.CO;2.

Cotton, R., S. Osborne, Z. Ulanowski, E. Hirst, P. H. Kaye, and R. S. Greenaway, 2010: The ability of the Small Ice Detector (SID2) to characterize cloud particle and aerosol morphologies obtained during flights of the FAAM BAe146 research aircraft. *J. Atmos. Oceanic Technol.*, **27**, 290–303, doi:10.1175/2009JTECHA1282.1.

——, and Coauthors, 2013: The effective density of small ice particles obtained from in situ aircraft observations of mid-latitude cirrus. *Quart. J. Roy. Meteor. Soc.*, **139**, 1923–1934, doi:10.1002/qj.2058.

Davis, S. M., A. G. Hallar, and L. M. Avallone, 2007: Measurement of total water with a tunable diode laser hygrometer: Inlet analysis, calibration procedure, and ice water content determination. *J. Atmos. Oceanic Technol.*, **24**, 463–475, doi:10.1175/JTECH1975.1.

Davison, C. R., J. D. MacLeod, and J. W. Strapp, 2009: Naturally aspirating isokinetic total water content probe: Evaporator design and testing. *First AIAA Atmospheric and Space Environments Conf.*, San Antonio, TX, AIAA, AIAA-2009-3861.

[Available online at https://arc.aiaa.org/doi/pdf/10.2514/6.2009-3861.]

——, T. P. Ratvasky, and L. E. Lilie, 2011: Naturally aspirating isokinetic total water content probe: Wind tunnel test results and design modifications. SAE Tech. Paper 2011-38-0036, 14 pp., doi:10.4271/2011-38-0036.

Emery, E., D. R. Miller, S. R. Plaskon, J. W. Strapp, and L. Lillie, 2004: Ice particle impact on cloud water content instrumentation. NASA Tech. Note, NASA/TM-2004-212964, 12 pp.

Field, P. R., R. Wood, P. R. A. Brown, P. H. Kaye, E. Hirst, R. Greenaway, and J. A. Smith, 2003: Ice particle interarrival times measured with a fast FSSP. *J. Atmos. Oceanic Technol.*, **20**, 249–261, doi:10.1175/1520-0426(2003)020<0249:IPITMW>2.0.CO;2.

——, A. J. Heymsfield, and A. Bansemer, 2006: Shattering and particle interarrival times measured by optical array probes in ice clouds. *J. Atmos. Oceanic Technol.*, **23**, 1357–1370, doi:10.1175/JTECH1922.1.

Fugal, J., and R. Shaw, 2009: Cloud particle size distributions measured with an airborne digital in-line holographic instrument. *Atmos. Meas. Tech.*, **2**, 259–271, doi:10.5194/amt-2-259-2009.

Gardiner, B. A., and J. Hallett, 1985: Degradation of in-cloud forward scattering spectrometer probe measurements in the presence of ice particles. *J. Atmos. Oceanic Technol.*, **2**, 171–180, doi:10.1175/1520-0426(1985)002<0171:DOICFS>2.0.CO;2.

Gayet, J.-F., G. Febvre, and H. Larsen, 1996: The reliability of the PMS FSSP in the presence of small ice crystals. *J. Atmos. Oceanic Technol.*, **13**, 1300–1310, doi:10.1175/1520-0426(1996)013<1300:TROTPF>2.0.CO;2.

——, O. Crepel, J. Fournol, and S. Oshchepkov, 1997: A new airborne polar nephelometer for the measurements of optical and microphysical cloud properties. Part 1: Theoretical design. *Ann. Geophys.*, **15**, 451–459, doi:10.1007/s00585-997-0451-1.

——, and Coauthors, 2002: Quantitative measurements of the microphysical and optical properties of cirrus clouds with four different in situ probes: Evidence of small ice crystals. *Geophys. Res. Lett.*, **29**, 2230, doi:10.1029/2001GL014342.

Gerber, H., B. Arends, and A. Ackerman, 1994: New microphysics sensor for aircraft use. *Atmos. Res.*, **31**, 235–252, doi:10.1016/0169-8095(94)90001-9.

——, C. H. Twohy, B. Gandrud, A. Heymsfield, G. McFarquhar, P. Demott, and D. Rogers, 1998: Measurements of wave-cloud microphysical properties made with two new aircraft cloud probes. *Geophys. Res. Lett.*, **25**, 1117–1120, doi:10.1029/97GL03310.

——, Y. Takano, T. J. Garrett, and P. V. Hobbs, 2000: Nephelometer measurements of the asymmetry parameter, volume extinction coefficient, and backscatter ratio in Arctic clouds. *J. Atmos. Sci.*, **57**, 3021–3034, doi:10.1175/1520-0469(2000)057<3021:NMOTAP>2.0.CO;2.

Glen, A., and S. D. Brooks, 2013: A new method for measuring optical scattering properties of atmospherically relevant dusts using the Cloud and Aerosol Spectrometer with Polarization (CASPOL). *Atmos. Chem. Phys.*, **13**, 1345–1356, doi:10.5194/acp-13-1345-2013.

Hallett, J., 2003: Measurement in the atmosphere. *Handbook of Weather, Climate and Water: Dynamics, Climate, Physical Meteorology, Weather Systems, and Measurements*, T. D. Potter and B. R. Colman, Eds., Wiley-Interscience, 711–720.

Heymsfield, A. J., 2007: On measurements of small ice particles in clouds. *Geophys. Res. Lett.*, **34**, L23812, doi:10.1029/2007GL030951.

——, and G. M. McFarquhar, 1996: High albedos of cirrus in the tropical Pacific warm pool: Microphysical interpretations from CEPEX and from Kwajalein, Marshall Islands. *J. Atmos. Sci.*, **53**, 2424–2451, doi:10.1175/1520-0469(1996)053<2424:HAOCIT>2.0.CO;2.

——, and Coauthors, 2017: Cirrus clouds. *Ice Formation and Evolution in Clouds and Precipitation: Measurement and Modeling Challenges*, *Meteor. Monogr.*, No. 58, Amer. Meteor. Soc., doi:10.1175/AMSMONOGRAPHS-D-16-0010.1.

Hirst, E., P. H. Kaye, R. S. Greenaway, P. Field, and D. W. Johnson, 2001: Discrimination of micrometre-sized ice and super-cooled droplets in mixed-phase cloud. *Atmos. Environ.*, **35**, 33–47, doi:10.1016/S1352-2310(00)00377-0.

Hovenac, E. A., and E. D. Hirleman, 1991: Use of rotating pinholes and reticles for calibration of cloud droplet instrumentation. *J. Atmos. Oceanic Technol.*, **8**, 166–171, doi:10.1175/1520-0426(1991)008<0166:UORPAR>2.0.CO;2.

Jackson, R. C., G. M. McFarquhar, J. Stith, M. Beals, R. A. Shaw, J. Jensen, J. Fugal, and A. Korolev, 2014: An assessment of the impact of antishattering tips and artifice removal techniques on cloud ice size distributions measured by the 2D cloud probe. *J. Atmos. Oceanic Technol.*, **31**, 2567–2590, doi:10.1175/JTECH-D-13-00239.1.

Järvinen, E., and Coauthors, 2016: Quasispherical ice in convective clouds. *J. Atmos. Sci.*, **73**, 3885–3910, doi:10.1175/JAS-D-15-0365.1.

Jensen, J., and H. Granek, 2002: Optoelectronic simulation of the PMS 260X optical array probe and application to drizzle in a marine stratocumulus. *J. Atmos. Oceanic Technol.*, **19**, 568–585, doi:10.1175/1520-0426(2002)019<0568:OSOTPO>2.0.CO;2.

Johnson, A., S. Lasher-Trapp, A. Bansemer, Z. Ulanowski, and A. J. Heymsfield, 2014: Difficulties in early ice detection with the Small Ice Detector-2 HIAPER (SID-2H) in maritime cumuli. *J. Atmos. Oceanic Technol.*, **31**, 1263–1275, doi:10.1175/JTECH-D-13-00079.1.

Kaye, P. H., and Coauthors, 2008: Classifying atmospheric ice crystals by spatial light scattering. *Opt. Lett.*, **33**, 1545–1547, doi:10.1364/OL.33.001545.

King, W. D., 1984: Air flow and particle trajectories around aircraft fuselages. I: Theory. *J. Atmos. Oceanic Technol.*, **1**, 5–13, doi:10.1175/1520-0426(1984)001<0005:AFAPTA>2.0.CO;2.

——, D. A. Parkin, and R. J. Handsworth, 1978: A hot-wired liquid water device having fully calculable response characteristics. *J. Appl. Meteor.*, **17**, 1809–1813, doi:10.1175/1520-0450(1978)017<1809:AHWLWD>2.0.CO;2.

——, D. E. Turvey, D. Williams, and D. J. Llewellyn, 1984: Air flow and particle trajectories around aircraft fuselages. II: Measurements. *J. Atmos. Oceanic Technol.*, **1**, 14–21, doi:10.1175/1520-0426(1984)001<0014:AFAPTA>2.0.CO;2.

Knollenberg, R., 1970: The optical array: An alternative to scattering or extinction for airborne particle size determination. *J. Appl. Meteor.*, **9**, 86–103, doi:10.1175/1520-0450(1970)009<0086:TOAAAT>2.0.CO;2.

——, 1976: Three new instruments for cloud physics measurements: The 2-D spectrometer probe, the forward scattering spectrometer probe, and the active scattering aerosol spectrometer. Preprints, *Int. Conf. on Cloud Physics*, Boulder, CO, Amer. Meteor. Soc., 554–561.

——, 1981: Techniques for probing cloud microstructure. *Clouds, Their Formation, Optical Properties and Effects*, P. V. Hobbs and A. Deepak, Eds., Academic Press, 15–91.

Korolev, A. V., 2007: Reconstruction of the sizes of spherical particles from their shadow images. Part I: Theoretical

considerations. *J. Atmos. Oceanic Technol.*, **24**, 376–389, doi:10.1175/JTECH1980.1.

——, and B. Sussman, 2000: A technique for habit classification of cloud particles. *J. Atmos. Oceanic Technol.*, **17**, 1048–1057, doi:10.1175/1520-0426(2000)017<1048:ATFHCO>2.0.CO;2.

——, and G. A. Isaac, 2005: Shattering during sampling by OAPs and HVPS. Part I: Snow particles. *J. Atmos. Oceanic Technol.*, **22**, 528–542, doi:10.1175/JTECH1720.1.

——, and P. R. Field, 2015: Assessment of the performance of the inter-arrival time algorithm to identify ice shattering artifacts in cloud particle probe measurements. *Atmos. Meas. Tech.*, **8**, 761–777, doi:10.5194/amt-8-761-2015.

——, S. V. Kuznetsov, Y. E. Makarov, and V. S. Novikov, 1991: Evaluation of measurements of particle size and sample area from optical array probes. *J. Atmos. Oceanic Technol.*, **8**, 514–522, doi:10.1175/1520-0426(1991)008<0514:EOMOPS>2.0.CO;2.

——, J. W. Strapp, and G. A. Isaac, 1998a: Evaluation of the accuracy of PMS Optical Array Probes. *J. Atmos. Oceanic Technol.*, **15**, 708–720, doi:10.1175/1520-0426(1998)015<0708:EOTAOP>2.0.CO;2.

——, ——, ——, and A. N. Nevzorov, 1998b: The Nevzorov airborne hot-wire LWC–TWC probe: Principle of operation and performance characteristics. *J. Atmos. Oceanic Technol.*, **15**, 1495–1510, doi:10.1175/1520-0426(1998)015<1495:TNAHWL>2.0.CO;2.

——, E. F. Emery, J. W. Strapp, S. G. Cober, G. A. Isaac, M. Wasey, and D. Marcotte, 2011: Small ice particles in tropospheric clouds: Fact or artifact? Airborne Icing Instrumentation Evaluation experiment. *Bull. Amer. Meteor. Soc.*, **92**, 967–973, doi:10.1175/2010BAMS3141.1.

——, ——, ——, ——, and ——, 2013a: Quantification of the effects of shattering on airborne ice particle measurements. *J. Atmos. Oceanic Technol.*, **30**, 2527–2553, doi:10.1175/JTECH-D-13-00115.1.

——, J. A. Strapp, G. A. Isaac, and E. Emery, 2013b: Improved airborne hot-wire measurements of ice water content in clouds. *J. Atmos. Oceanic Technol.*, **30**, 2121–2131, doi:10.1175/JTECH-D-13-00007.1.

——, A. Shavkov, and H. Barker, 2014: Calibration and performance of the cloud extinction probe. *J. Atmos. Oceanic Technol.*, **31**, 326–345, doi:10.1175/JTECH-D-13-00020.1.

Krämer, M., and A. Afchine, 2004: Sampling characteristics of inlets operated at low U/U0 ratios: New insights from computational fluid dynamics (CFX) modeling. *J. Aerosol Sci.*, **35**, 683–694, doi:10.1016/j.jaerosci.2003.11.011.

——, and Coauthors, 2016: A microphysics guide to cirrus clouds—Part 1: Cirrus types. *Atmos. Chem. Phys.*, **16**, 3463–3483, doi:10.5194/acp-16-3463-2016.

Lance, S., 2012: Coincidence errors in a cloud droplet probe (CDP) and a cloud and aerosol spectrometer (CAS), and the improved performance of a modified CDP. *J. Atmos. Oceanic Technol.*, **29**, 1532–1541, doi:10.1175/JTECH-D-11-00208.1.

——, C. A. Brock, D. Rogers, and J. A. Gordon, 2010: Water droplet calibration of the cloud droplet probe (CDP) and in-flight performance in liquid, ice and mixed-phase clouds during ARCPAC. *Atmos. Meas. Tech.*, **3**, 1683–1706, doi:10.5194/amt-3-1683-2010.

Lawson, R. P., 2011: Effects of ice particles shattering on the 2D-S probe. *Atmos. Meas. Tech.*, **4**, 1361–1381, doi:10.5194/amt-4-1361-2011.

——, R. E. Stewart, and L. J. Angus, 1998: Observations and numerical simulations of the origin and development of very large snowflakes. *J. Atmos. Sci.*, **55**, 3209–3229, doi:10.1175/1520-0469(1998)055<3209:OANSOT>2.0.CO;2.

——, B. A. Baker, C. G. Schmitt, and T. L. Jensen, 2001: An overview of microphysical properties of Arctic clouds observed in May and July during FIRE ACE. *J. Geophys. Res.*, **106**, 14 989–15 014, doi:10.1029/2000JD900789.

——, D. O'Connor, P. Zmarzly, K. Weaver, B. A. Baker, Q. Mo, and H. Jonsson, 2006: The 2DS (stereo) probe: Design and preliminary tests of a new airborne, high speed, high-resolution particle imaging probe. *J. Atmos. Oceanic Technol.*, **23**, 1462–1471, doi:10.1175/JTECH1927.1.

——, S. Woods, and H. Morrison, 2015: The microphysics of ice and precipitation development in tropical cumulus clouds. *J. Atmos. Sci.*, **72**, 2429–2445, doi:10.1175/JAS-D-14-0274.1.

Luebke, A. E., L. M. Avallone, C. Schiller, J. Meyer, C. Rolf, and M. Krämer, 2013: Ice water content of Arctic, midlatitude, and tropical cirrus—Part 2: Extension of the database and new statistical analysis. *Atmos. Chem. Phys.*, **13**, 6447–6459, doi:10.5194/acp-13-6447-2013.

McFarquhar, G. M., J. Um, M. Freer, D. Baumgardner, G. L. Kok, and G. Mace, 2007: Importance of small ice crystals to cirrus properties: Observations from the Tropical Warm Pool International Cloud Experiment (TWP-ICE). *Geophys. Res. Lett.*, **34**, L13803, doi:10.1029/2007GL029865.

——, ——, and R. C. Jackson, 2013: Small cloud particle shapes in mixed-phase clouds. *J. Appl. Meteor. Climatol.*, **52**, 1277–1293, doi:10.1175/JAMC-D-12-0114.1.

——, and Coauthors, 2017: Data analysis, interpretation, and presentation of in situ measurements. *Ice Formation and Evolution in Clouds and Precipitation: Measurement and Modeling Challenges*, *Meteor. Monogr.*, No. 58, Amer. Meteor. Soc., doi:10.1175/AMSMONOGRAPHS-D-16-0007.1.

Meyer, J., 2012: *Ice Crystal Measurements with the New Particle Spectrometer NIXE-CAPS*. Energy and Environment Series, Vol. 160, Jülich Research Centre, 132 pp.

——, and Coauthors, 2015: Two decades of water vapor measurements with the FISH fluorescence hygrometer: A review. *Atmos. Chem. Phys.*, **15**, 8521–8538, doi:10.5194/acp-15-8521-2015.

Nicholls, S., J. Leighton, and R. Barker, 1990: A new fast response instrument for measuring total water content from aircraft. *J. Atmos. Oceanic Technol.*, **7**, 706–718, doi:10.1175/1520-0426(1990)007<0706:ANFRIF>2.0.CO;2.

Noone, K. J., J. A. Ogren, J. Heintzenberg, R. J. Charlson, and D. S. Covert, 1988: Design and calibration of a counterflow virtual impactor for sampling of atmospheric fog and cloud droplets. *Aerosol Sci. Technol.*, **8**, 235–244, doi:10.1080/02786828808959186.

Norment, H., 1985: Calculation of water drop trajectories to and about arbitrary three-dimensional lifting and nonlifting bodies in potential airflow. NASA Tech. Rep. NASA-CR-3935, 168 pp. [Available online at https://ntrs.nasa.gov/archive/nasa/casi.ntrs.nasa.gov/19870002261.pdf.]

——, 1988: Three-dimensional trajectory analysis of two drop sizing instruments: PMS-OAP and PMS-FSSP. *J. Atmos. Oceanic Technol.*, **5**, 743–756, doi:10.1175/1520-0426(1988)005<0743:TDTAOT>2.0.CO;2.

Porcheron, E., P. Lemaitre, J. Van Beeck, R. Vetrano, M. Brunel, and G. Grehan, 2015: Development of a spectrometer for airborne measurement of droplet sizes in clouds. *J. Eur. Opt. Soc. Rapid Publ.*, **10**, 15030, doi:10.2971/jeos.2015.15030.

Schiller, C., M. Krämer, A. Afchine, N. Spelten, and N. Sitnikov, 2008: Ice water content of Arctic, midlatitude, and tropical cirrus. *J. Geophys. Res.*, **113**, D24208, doi:10.1029/2008JD010342.

Schnaiter, M., and Coauthors, 2016: Cloud chamber experiments on the origin of ice crystal surface roughness in cirrus clouds. *Atmos. Chem. Phys.*, **16**, 5091–5110, doi:10.5194/acp-16-5091-2016.

Schön, R., and Coauthors, 2011: Particle habit imaging using incoherent light: A first step toward a novel instrument for cloud microphysics. *J. Atmos. Oceanic Technol.*, **28**, 493–512, doi:10.1175/2011JTECHA1445.1.

Schwarzenboeck, A., G. Mioche, A. Armetta, A. Herber, and J.-F. Gayet, 2009: Response of the Nevzorov hot wire probe in clouds dominated by droplet conditions in the drizzle size range. *Atmos. Meas. Tech.*, **2**, 779–788, doi:10.5194/amt-2-779-2009.

Ström, J., and J. Heintzenberg, 1994: Water vapor, condensed water, and crystal concentration in orographically influenced cirrus clouds. *J. Atmos. Sci.*, **51**, 2368–2383, doi:10.1175/1520-0469(1994)051<2368:WVCWAC>2.0.CO;2.

Twohy, C. H., and D. Rogers, 1993: Airflow and water drop trajectories at instrument sampling points around the Beechcraft King Air and Lockheed Electra. *J. Atmos. Oceanic Technol.*, **10**, 566–578, doi:10.1175/1520-0426(1993)010<0566:AAWDTA>2.0.CO;2.

——, A. J. Schanot, and W. A. Cooper, 1997: Measurement of condensed water content in liquid and ice clouds using an airborne counterflow virtual impactor. *J. Atmos. Oceanic Technol.*, **14**, 197–202, doi:10.1175/1520-0426(1997)014<0197:MOCWCI>2.0.CO;2.

——, J. W. Strapp, and M. Wendisch, 2003: Performance of a counterflow virtual impactor in the NASA Icing Research Tunnel. *J. Atmos. Oceanic Technol.*, **20**, 781–790, doi:10.1175/1520-0426(2003)020<0781:POACVI>2.0.CO;2.

Ulanowski, Z., and M. Schnaiter, 2011: UV and visible light scattering and absorption measurements on aerosols in the laboratory. *Fundamentals and Applications of Aerosol Spectroscopy*, J. P. Reid and R. Signorell, Eds., CRC Press, 243–268.

——, P. Connolly, M. Flynn, M. Gallagher, A. J. M. Clarke, and E. Hesse, 2004: Using ice crystal analogues to validate cloud ice parameter retrievals from the CPI ice spectrometer. *Proc. 14th Int. Conf. on Clouds and Precipitation*, Bologna, Italy, ICCP, 1175–1178.

——, E. Hesse, P. Kaye, and A. J. Baran, 2006: Light scattering by complex ice-analogue crystals. *J. Quant. Spectrosc. Radiat. Transfer*, **100**, 382–392, doi:10.1016/j.jqsrt.2005.11.052.

——, E. Hirst, P. H. Kaye, and R. Greenaway, 2012: Retrieving the size of particles with rough and complex surfaces from two-dimensional scattering patterns. *J. Quant. Spectrosc. Radiat. Transfer*, **113**, 2457–2464, doi:10.1016/j.jqsrt.2012.06.019.

——, P. H. Kaye, E. Hirst, R. S. Greenaway, R. J. Cotton, E. Hesse, and C. T. Collier, 2014: Incidence of rough and irregular atmospheric ice particles from Small Ice Detector 3 measurements. *Atmos. Chem. Phys.*, **14**, 1649–1662, doi:10.5194/acp-14-1649-2014.

Um, J., and G. M. McFarquhar, 2015: Formation of atmospheric halos and applicability of geometric optics for calculating single-scattering properties of hexagonal ice crystals: Impacts of aspect ratio and ice crystal size. *J. Quant. Spectrosc. Radiat. Transfer*, **165**, 134–152, doi:10.1016/j.jqsrt.2015.07.001.

Vidaurre, G., and J. Hallett, 2009: Particle impact and breakup in aircraft measurements. *J. Atmos. Oceanic Technol.*, **26**, 972–983, doi:10.1175/2008JTECHA1147.1.

Vochezer, P., E. Järvinen, R. Wagner, P. Kupiszewski, T. Leisner, and M. Schnaiter, 2016: In situ characterization of mixed phase clouds using the Small Ice Detector and the Particle Phase Discriminator. *Atmos. Meas. Tech.*, **9**, 159–177, doi:10.5194/amt-9-159-2016.

Weinstock, E. M., and Coauthors, 2006: Measurements of the total water content of cirrus clouds. Part I: Instrument details and calibration. *J. Atmos. Oceanic Technol.*, **23**, 1397–1409, doi:10.1175/JTECH1928.1.

Wendisch, M., and J. L. Brenguier, Eds., 2013: *Airborne Measurements for Environmental Research: Methods and Instruments*. Wiley and Sons, 641 pp.

——, T. Garrett, and J. Strapp, 2002: Wind tunnel tests of the airborne PVM-100A response to large droplets. *J. Atmos. Oceanic Technol.*, **19**, 1577–1584, doi:10.1175/1520-0426(2002)019<1577:WTTOTA>2.0.CO;2.

——, and Coauthors, 2004: Aircraft particle inlets: State-of-the-art and future needs. *Bull. Amer. Meteor. Soc.*, **85**, 89–91, doi:10.1175/BAMS-85-1-89.

Wu, W., and G. McFarquhar, 2016: On the impacts of different definitions of maximum dimension for nonspherical particles recorded by 2D imaging probes. *J. Atmos. Oceanic Technol.*, **33**, 1057–1072,doi:10.1175/JTECH-D-15-0177.1.

Yang, P., and K. N. Liou, 1998: Single-scattering properties of complex ice crystals in terrestrial atmosphere. *Contrib. Atmos. Phys.*, **71**, 223–248.

——, L. Bi, B. A. Baum, K.-N. Liou, G. W. Kattawar, M. I. Mishchenko, and B. Cole, 2013: Spectrally consistent scattering, absorption, and polarization properties of atmospheric ice crystals at wavelengths from 0.2 to 100 μm. *J. Atmos. Sci.*, **70**, 330–347, doi:10.1175/JAS-D-12-039.1.